Contrib Mineral Petrol (1992) 111:203–221

Contributions to Mineralogy and Petrology

Oxygen and hydrogen isotope evidence for meteoric water infiltration during mylonitization and uplift in the Ruby Mountains-East Humboldt Range core complex, Nevada

Henry C. Fricke*, Stephen M. Wickham, and James R. O'Neil

Department of the Geophysical Sciences and Enrico Fermi Institute, University of Chicago, 5734 South Ellis Avenue, Chicago, IL 60637-1472, USA
Department of Geological Sciences, University of Michigan, 1006 C.C. Little Building, Ann Arbor, MI 48109-1063, USA

Received July 9, 1991 / Accepted February 10, 1992

Abstract. Stable isotope analyses of rocks and minerals associated with the detachment fault and underlying mylonite zone exposed at Secret Creek gorge and other localities in the Ruby-East Humboldt Range metamorphic core complex in northeastern Nevada provide convincing evidence for meteoric water infiltration during mylonitization. Whole-rock $\delta^{18}O$ values of the lower plate quartzite mylonites ($\geq 95\%$ modal quartz) have been lowered by up to 10 per mil compared with structurally lower, compositionally similar, unmylonitized material. Biotite from these rocks has δD values ranging from -125 to -175, compared to values of -55 to -70 in biotite from unmylonitized rocks. Mylonitized leucogranites have large disequilibrium oxygen isotope fractionations ($\Delta_{quartz\text{-}feldspar}$ up to ~ 8 per mil) relative to magmatic values ($\Delta_{quartz\text{-}feldspar}$ ~ 1 to 2 per mil). Meteoric water is the only major oxygen and hydrogen reservoir with an isotopic composition capable of generating the observed values. Fluid inclusion water from unstrained quartz in silicified breccia has a δD value of -119 which provides a plausible estimate of the δD of the infiltrating fluid, and is similar to the isotopic composition of present-day and Tertiary local meteoric water. The quartzite mylonite biotites would have been in equilibrium with such a fluid at temperatures of 480–620° C, similar to independent estimates of the temperature of mylonitization. The relatively high temperatures required for isotopic exchange between quartz and water, the occurrence of fluid inclusion trails and deformed veins in quartzite mylonites, and the spatial association of the low-^{18}O, low-D rocks with the shear zone all constrain isotopic exchange to the mylonitic (plastic) deformation event. These observations suggest that a significant amount of meteoric water infiltrated the shear zone during mylonitization to depths of at least 5 to 10 km below the surface. The depth of penetration of meteoric fluids into the lower plate mylonites was *at least* 70 meters below the detachment fault. In contrast, the upper-plate unmylonitized fault slices are dominated by brittle fracture and are often intensely veined (carbonates) or silicified (volcanic rocks and breccias). The fluids associated with the veining and silicification were also meteoric as evidenced by low $\delta^{18}O$ values of the veins, which are often 10 per mil lower than the adjacent carbonate matrix, and the exceptionally low $\delta^{18}O$ values (down to -4.4) of the breccias. Several previous studies have documented the infiltration of meteoric fluids into the brittley deformed upper plate rocks of core complexes, but this study provides convincing evidence that surface fluids have penetrated lower plate rocks undergoing plastic deformation. It is proposed that infiltration took place as the shear zone began the transition from plastic flow to brittle fracture while the lower plate rocks were being uplifted. During this period, plastic flow and brittle fracture were operating simultaneously, perhaps allowing upper plate meteoric fluids to be seismically pumped down into the lower plate mylonites.

Introduction

The movement of fluids through the crust exerts profound influence on processes such as heat and mass transport, and mechanical deformation. Many questions remain concerning the sources of fluids, the driving forces behind flow, and the overall geometry of fluid movement. Several recently published geochemical and isotopic studies indicate that shear zones are particularly good environments for fluid flow at various crustal depths (e.g. Kerrich and Hyndman 1986; Kerrich and Rehrig 1987; LaTour and Barnett 1987; McCaig 1988; McCaig et al. 1990; Smith et al. 1991). This study supports this conclusion by presenting evidence for extensive interaction of meteoric water with the mylonitized rocks of a shear zone during extensional deformation.

* Present address: Department of Geological Sciences, University of Michigan, 1006 C.C. Little Building, Ann Arbor, MI 48109-1063, USA

Offprint requests to: H.C. Fricke

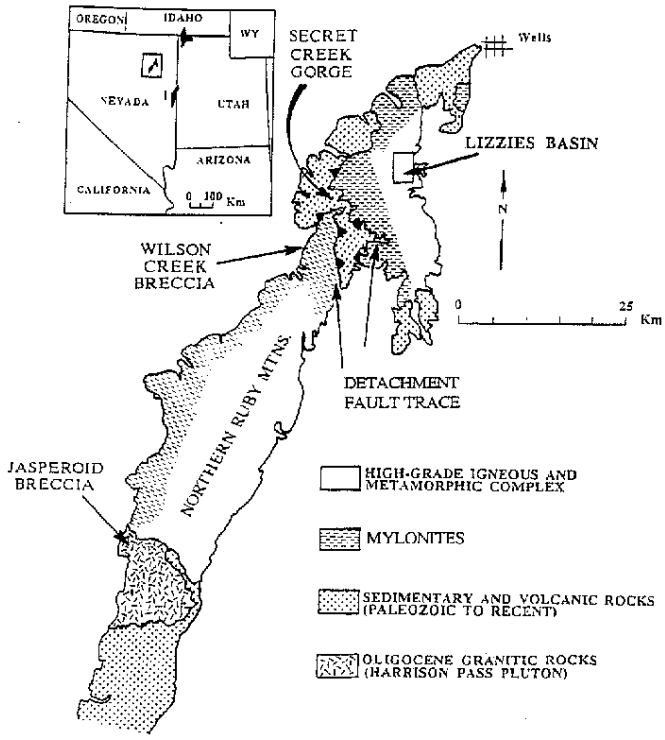

Fig. 1. The location of the area studied in north-eastern Nevada and the simplified geology of the Ruby-East Humboldt Range core complex. A mylonite overprint occurs through much of the upper structural levels of the high-grade igneous and metamorphic lower plate rocks (*dash pattern*) becoming more intense close to the low angle detachment fault which separates them from overlying low-grade rocks. This transition from lower plate to upper plate is very well exposed at Secret Creek gorge (see also Fig. 3). The deepest structural levels in the entire area are exposed at Lizzies Basin, and two occurrences of silicified breccia sheets at Wilson Creek and near Harrison Pass (marked by jasperoid breccia) are also shown. The inset map also marks the location of other nearby core complexes including the Snake Range in eastern Nevada and the Grouse Creek-Albion Mountains in northwestern Utah and southern Idaho

Because of excellent exposure over a range of structural levels and the very distinctive oxygen and hydrogen isotope signature of the infiltrating fluid, we have been able to resolve the geometry of fluid infiltration in a shear zone environment in unprecedented detail. In particular, we have been able to document the infiltration of fluids into the rocks of the plastically deforming shear zone *itself*, in addition to structurally higher cataclastic breccia zones.

The area studied forms part of the Ruby Mountains-East Humboldt Range in northeastern Nevada (Fig. 1). This metamorphic core complex comprises two distinct structural components: a structurally deep footwall of high-grade metamorphic and igneous rocks, which is separated by a shallowly dipping detachment fault from low-grade to unmetamorphosed hanging-wall sediments and volcanic rocks. Rock units directly below the detachment fault have been extensively mylonitized over a zone several hundreds of meters thick. Extensional displacement along the shear zone-detachment fault system resulted in the removal of 11–12 km of overburden in order to expose these rocks at the surface and juxtapose them against the low-grade rocks. Much of the mylonitization and uplift occurred over a relatively short time interval during the middle Tertiary (Dokka et al. 1986). Microstructural examination of the mylonites also suggests relatively rapid uplift rates on the order of kilometers per million years (Hacker et al. 1990).

Rapid uplift during extensional deformation may generate conditions favorable for meteoric-hydrothermal activity because rapidly uplifted high-grade rocks may be anomalously hot. This could arise if they were exhumed faster than they could cool conductively to ambient temperatures (England and Richardson 1977; Koons 1987). They therefore function as "heat engines" that can drive hydrothermal circulation, in the same way as magmas or cooling plutons provide the requisite heat energy for hydrothermal systems centered on high level igneous intrusions (Taylor 1977). Furthermore, extensional deformation can generate steep, deeply-penetrating fracture systems that will facilitate downward movement of surface water. We have tested this hypothesis by looking for evidence of meteoric fluid interaction within the shear zone and detachment fault system in the Ruby-East Humboldt Range. Our preliminary results indicate that meteoric fluids extensively infiltrated the shear zone, resulting in profound ^{18}O-depletion even in quartzite mylonites, an effect which appears to decrease in intensity with increasing structural depth.

Geological setting

Regional geology

The Ruby Mountains-East Humboldt Range of northeastern Nevada is a north-south trending horst comprising mostly high-grade crystalline rocks and miogeoclinal sediments (Snoke and Howard 1984). Exposed in its deeper structural levels are amphibolite facies metasedimentary and igneous gneisses intruded by a variety of granitoids. Structurally above the igneous and metamorphic complex and separated from it by a low-angle detachment fault, is a cover terrane comprising fault-bounded blocks of low-grade or unmetamorphosed rocks (Figs. 1 and 2). A variably penetrative, locally mylonitic deformation is superimposed on a large part of the igneous and metamorphic complex (lower plate), with mylonites being especially well developed along the western side of the range towards the top of the lower-plate rocks (see Fig. 1). The mylonite fabric deforms and therefore postdates the regional metamorphic assemblages generated in the lower-plate rocks; however, the grade of mylonitization was higher than greenschist facies as biotite was stable during dynamic recrystallization (Snoke 1980; Lister and Snoke 1984; Dallmeyer et al. 1986). Hurlow et al. (1991) estimate pressures of 3–4 kbar and temperatures of 580–620° C for part of the mylonitization. The mylonite zone dips at relatively low angles and is cut by numerous low- and high-angle brittle normal faults, particularly in its upper part. A series of low-angle listric normal faults, some of which sole into mylonitic layers, separate the mylonites from the overlying unmetamorphosed upper plate rocks. Volcanic rocks that have been dated at 15 Ma are involved in the low-angle normal faulting, and some of the tectonism must therefore be younger than this age (Dallmeyer et al. 1986).

In general, the structural chronology represented by the detachment fault zone and its associated mylonites is a transition from dominantly ductile lower plate processes to dominantly brittle up-

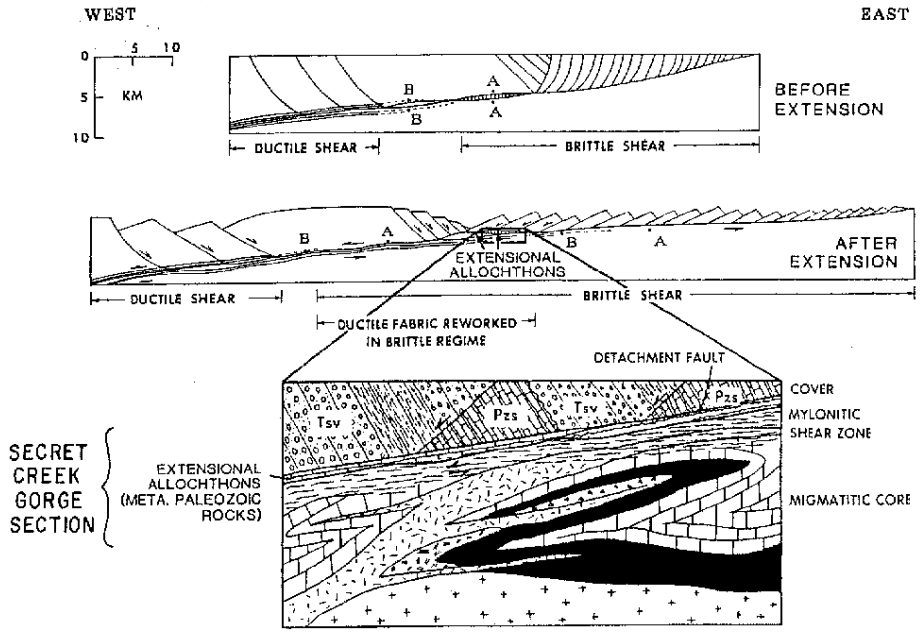

Fig. 2. A schematic cross section (after Dokka et al. 1986) through the Ruby-East Humboldt core complex illustrating the tectonic evolution during Tertiary extension, and the resulting structural relations between the upper and lower plate rocks (see Dokka et al. (1986) for complete lithological legend)

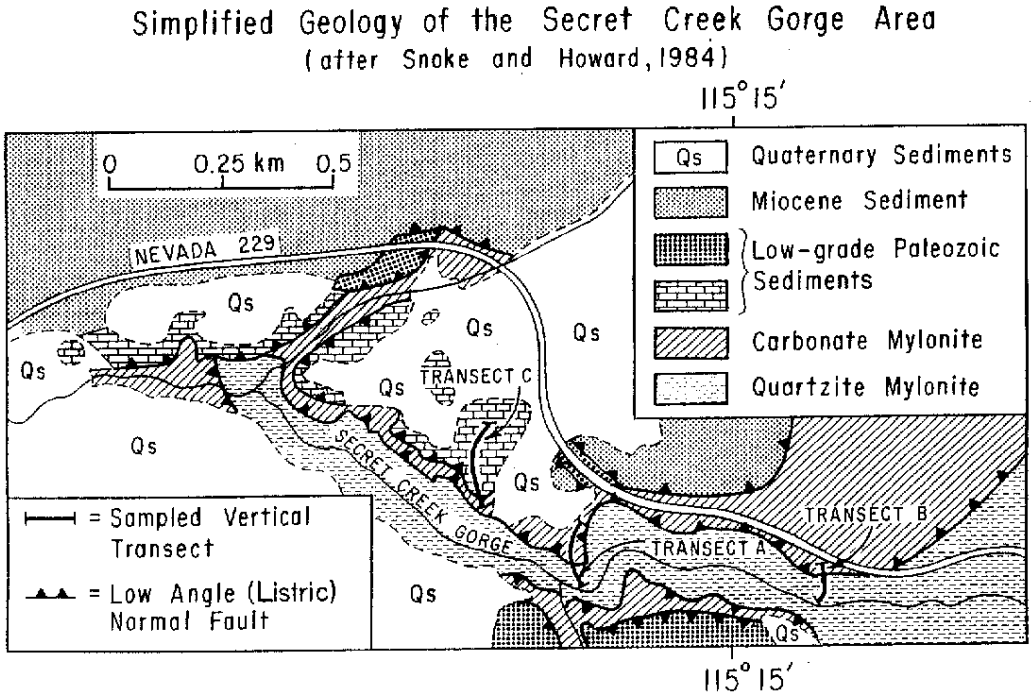

Fig. 3. A detailed map of the Secret Creek gorge area (modified after Snoke and Howard 1984) showing the numerous low-angle listric normal faults associated with the shear zone-detachment fault system, all of them placing younger rocks on older. We define the fault separating the Horse Creek assemblage (carbonate mylonite) from overlying units as the "main detachment fault" because it separates the low-grade, unmylonitized fault slices, from the high-grade, mylonitized Horse Creek and quartzite-schist and thus forms the boundary between upper and lower plate rocks in this area. The three sampled transects (shown as *heavy lines*) correspond to vertical transitions from low-grade upper plate to lower plate mylonites exposed in the walls of Secret Creek gorge. The Guilmette and underlying dolomitic carbonate are represented by the *brick pattern*, the Pennsylvanian Diamond Peak by the *heavy stipple* and the Miocene Humboldt Formation by the *light stipple*

per plate processes, although textures (such as mylonitized quartz veins) indicate that both could have been approximately contemporaneous for limited periods of time. In all cases within the transition zone between the lower plate and the upper plate, faults emplace rocks from higher structural levels on deeper, higher-grade rocks. This structural style has been described at numerous Cordilleran localities (e.g. Noble 1941; Wright and Troxel 1973; Rehrig and Reynolds 1980; Davis 1980) and reflects crustal extension which juxtaposes rock units with contrasting thermal histories (such as upper- and lower-plate lithologies) along low-angle normal

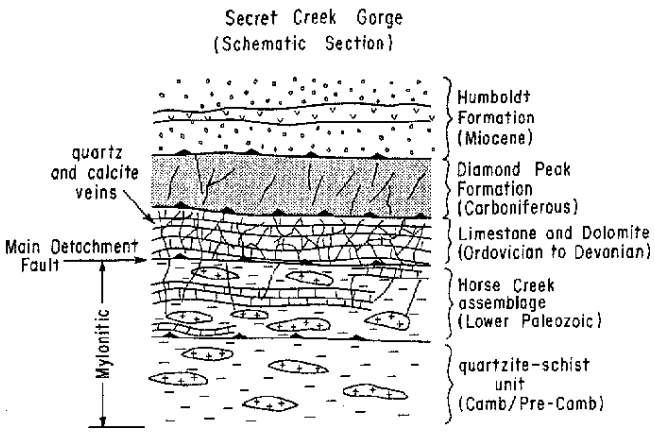

Fig. 4. Composite schematic section showing structural relations between rock units exposed in the Secret Creek gorge area. Low-grade Paleozoic to Cenozoic sediments and volcanic rocks overlie strongly mylonitized amphibolite facies rocks along the main detachment fault. All contacts between the different lithological units are low-angle listric normal faults. Leucogranite pods (cross pattern) occur throughout the high-grade units. The mylonites show little sign of late stage veining or cataclasis, whereas the upper plate rocks are extensively veined by quartz and calcite. No significant fault breccia zone occurs within the Secret Creek gorge section. The section is about 150 m thick in the Secret Creek gorge region

faults. These faults may have originally been active at high angles and subsequently been rotated into their current, subhorizontal attitude (Miller et al. 1983; Buck 1988), or they may originally have been developed at low angles (Yin 1989). A schematic section across the different structural levels exposed in the Ruby-East Humboldt Range is shown in Fig. 2 (see also Snoke 1980; Dallmeyer et al. 1986; Dokka et al. 1986).

Geology of Secret Creek gorge

The transition through the mylonites and low-angle normal faults from the lower plate to upper-plate rocks is exposed in various parts of the range, but the best and most easily accessible exposures are in the Secret Pass area, in particular at Secret Creek gorge at the northern end of the Ruby Mountains (see Figs. 1 and 3). This area was mapped by Snoke (1980), who gives a detailed description of the transition from the lower-plate metamorphic complex to low-grade, upper-plate Tertiary volcanic rocks and sediments. Figure 3 is a map of the Secret Creek gorge area and Fig. 4 shows a schematic section through the succession of units exposed. The stratigraphic age of the rocks ranges from the late Pre-Cambrian to the Miocene, with impure quartzite and schist intruded by abundant leucogranite pods being the lowest unit exposed (Snoke 1980; Snoke and Howard 1984). This is separated by a low-angle fault from overlying rocks of the Horse Creek assemblage, which comprise a diverse mixture of rock-types including calcite marble, calc-silicate gneiss and schist, leucogranite, granitic orthogneiss, and biotite-hornblende diorite. Both of these lowermost units are extensively mylonitized, complexly deformed, and cut by brittle and ductile normal faults. In some parts of the Secret Creek gorge section, unmylonitized fault-bounded slices of other metasedimentary miogeoclinal units such as the Ordovician Eureka Quartzite, various Ordovician to Devonian limestones and dolomites, Devonian Guilmette Formation (dominated by limestone), and the Pennsylvanian Diamond Peak Formation (dominated by coarse clastic sediments) rest on variably mylonitized Horse Creek lithologies and the quartzite schist unit. Overlying all these units and separated from them by another low-angle fault are unmetamorphosed sediments of the Miocene Humboldt Formation.

Petrography and sampling

Terminology

In this paper the term mylonite will be used to describe rocks in which "... the matrix minerals undergo extensive dynamic recrystallization ... and strong patterns of preferred crystallographic orientation typically develop" (Lister and Snoke 1984). Note that in this definition mylonites are not regarded as cataclastic rocks. While cataclastic processes may be involved during mylonitization, such as in coarse feldspars grains within a mylonitized granite, crystal-plastic deformation is the dominant strain accomodation mechanism. In the case of the quartzite mylonites at Secret Creek, the matrix quartz has undergone complete dynamic recrystallization and sub-grain elongation, thereby providing a plastic substrate within which feldspar and mica grains can rotate (Fig. 5a). Unlike mylonites associated with some other detachment faults (Kerrich and Hyndman 1986; Kerrich and Rehrig 1987; LaTour and Barnett 1987; Smith et al. 1991), the Secret Creek rocks have not been extensively texturally overprinted by low-temperature brittle deformation or "microbreccia" formation.

Quartzite mylonites (quartzite-schist unit)

The quartzofeldspathic metasediments in the footwall comprise quartzites and mica schists of Late Proterozoic or Early Paleozoic age, collectively known as the quartzite-schist unit. The quartzite mylonites which dominate the footwall rocks at Secret Creek are generally composed of quartz (90–97%) + feldspar (1–10%) + biotite (2–5%) with minor accessory muscovite and garnet. The exact composition is slightly variable, and some samples are more feldspathic or mica-rich than others. In the quartzites, the more resistant feldspar (and garnet when present) are cataclastically rotated within the dynamically recrystallized quartz matrix (quartz subgrains are 42–64 μm in length, with aspect ratios variable but sometimes exceeding 3:1; see also Hacker et al. 1990). Biotite is predominantly dark, fine-grained (10–30 μm), and is found in thin layers (50–75 μm thick) which define the main foliation, interspersed with quartz (see Fig. 5a). Muscovite porphyroclasts are less common, and usually take the form of relatively large (1.2–0.5 mm) mica "fish" that have also been variably rotated. Larger biotite grains also occur, but are less abundant than muscovite. Biotite is invariably fresh and unchloritized, suggesting that deformation occurred at elevated temperatures, probably >400° C.

In addition to plastic deformation, the quartzites show the effects of late stage brittle fracture, as evidenced by thin (25–75 μm) veins of quartz (±chlorite±muscovite) that crosscut the mylonite in some samples. In some cases this quartz has also been dynamically recrystallized and the veins deformed, and in others they have not. Many unfractured quartzite mylonites contain abundant 'healed' fractures, as evidenced by fluid inclusion trails in the quartz (see Fig. 5b). These also crosscut the mylonite. From these observations, we conclude that fracturing and mylonitization were approximately contemporaneous at some stage.

The quartz-rich metasediments are interlayered with sporadic micaceous pelitic schist units dominantly composed of fine-grained quartz, plagioclase, K-feldspar, muscovite, sillimanite, and biotite with plagioclase and garnet porphyroclasts (M.T. Peters, personal communication, 1991). Garnet, and possibly sillimanite, may be relict, pre-mylonite minerals, but the rest of the assemblage was stable under the conditions of mylonitization. These layers have a variable thickness ranging from several millimeters to meters, but are typically tens of centimeters thick.

Carbonate mylonites (Horse Creek assemblage)

The mylonitized carbonate metasediments are part of the Lower Paleozoic Horse Creek assemblage (Snoke 1980; Snoke and How-

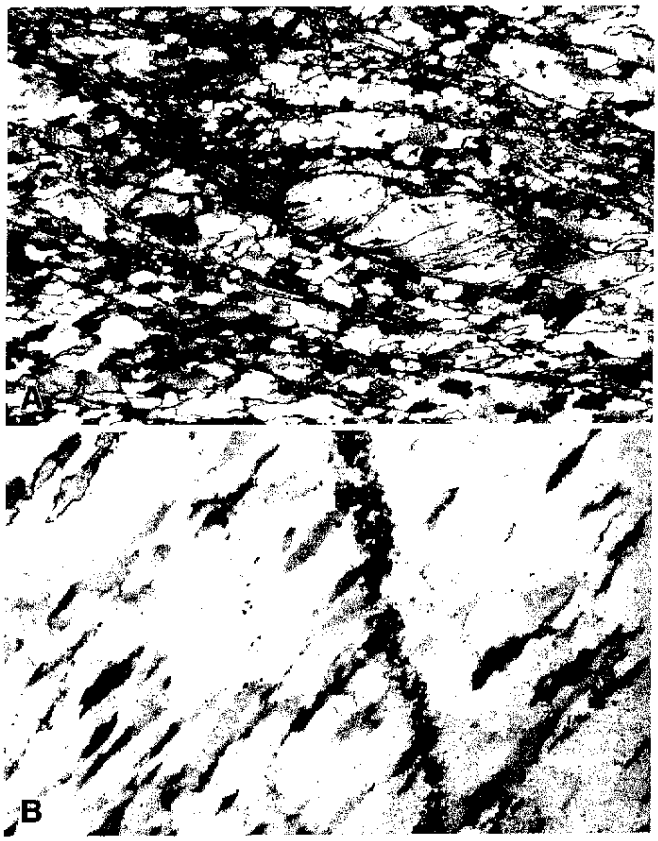

Fig. 5. A Photomicrograph of a Secret Pass quartzite S-C mylonite (2 mm by 2 mm). Note the elongated, recrystallized quartz subgrains, the compositional layers of fine-grained muscovite and biotite, and the muscovite and biotite porphyroclasts which have partially rotated within the quartz matrix. This photomicrograph shows only one of a variety of textural variations common in the quartzite mylonites at Secret Creek gorge. For a detailed description of these rocks see Lister and Snoke (1984). **B** Photomicrograph of a quartzite mylonite made up almost entirely of quartz (2 mm by 2 mm). Note the extreme quartz subgrain elongation as compared to Fig. 5a, and the occurrence of parallel fluid inclusion trails in the matrix quartz

ard 1984) and have been intensely deformed, showing extensive folding and dynamic recrystallization. This unit is composed predominantly of pure calcite marbles, interspersed with layers and boudins of calc-silicate gneiss and schist. Intrusive pods of leucogranite similar to those in the quartzite-schist unit are also common. Dynamic recrystallization is much more extreme in the marbles than in the gneissic layers, which comprise diopside and grossular-bearing assemblages similar to those described elsewhere in the East Humboldt Range (Peters and Wickham 1989). The latter have behaved as relatively rigid blocks within a plastically deforming carbonate matrix.

Leucogranite mylonites

The quartzites, mica-schists and carbonates are intruded by a suite of Mesozoic and/or Tertiary leucogranite pods (K-feldspar ~40%, plagioclase ~35%, quartz ~20%, muscovite 1–5%, ± biotite), which have also undergone mylonitization (Kistler et al. 1981; Wright and Snoke 1986), and have a typical thickness of tens of centimeters. The higher abundance and coarse grain size of feldspar in these rocks compared to the quartzites reduces the effects of mylonitization. Quartz is typically elongated or smeared out into millimeter scale ribbons, defining a strong foliation. Feldspar porphyroclasts are less strongly affected but may be rotated or brittley fractured. However, all phases including feldspar have undergone grain size reduction in local fine-grained layers of ultramylonite. In many cases the feldspar has undergone minor alteration to fine-grained white mica.

Hanging Wall (upper plate) fault slices

The unmylonitized fault slices lying structurally above the detachment fault (see Figs. 2 and 4) are not plastically deformed, but contain complicated fracture networks. The carbonate rocks structurally lowest within the hanging wall are Ordovician to Devonian low-grade dolomitic limestones, with a matrix comprising fine-grained grey carbonate (Snoke and Lush 1984). This unit is crosscut randomly and pervasively by quartz veins typically <2 mm thick. The Devonian Guilmette formation which overlies this is a low-grade grey metalimestone (Snoke and Lush 1984), with a regular pattern of steeply dipping, distinct, 2–3 mm-thick calcite veins occurring throughout and cutting the fault plane at high angles.

Above these units lie unmetamorphosed Pennsylvanian (Diamond Peak Formation) and Tertiary (Humboldt Formation) volcanic rocks and sediments, which are cut by high angle normal faults. At Secret Creek they are relatively undeformed except for brittle fracturing, but locally the Diamond Peak has been silicified, as evidenced by occurrences of jasper. The silicification is patchy but locally very intense.

Silicified rocks from the same structural level as the Secret Creek gorge exposure also occur at Wilson Creek about 10 km to the south (see Fig. 1 and Snoke 1980). The Wilson Creek breccia sheet contains clasts of a variety of lower plate lithologies, but some zones are foliated and contain flattened clasts; folds occur locally, suggesting that brittle and ductile deformation may have occurred approximately concurrently (Snoke 1980). This breccia sheet is similar to the silicified breccia sheet mapped in the range front by Willden and Kistler (1969) overlying the Harrison Pass Pluton in the central Ruby Mountains (see Fig. 1).

Sampling

Several vertical sampling traverses were made through the various low angle faults and into the underlying mylonite zone at Secret Creek gorge (Fig. 3). The data are given in Tables 1 and 2 together with sample location and petrographic information. The structural position of each quartzite-schist sample within the Secret Creek section, relative to the contact between this unit and the overlying Horse Creek assemblage, was also recorded (see Table 1). Poor exposure precluded such a precise location of the other samples. The traverses were aimed at detecting vertical and lateral mineralogical and oxygen isotope variations that may have resulted from fluid flow associated with the detachment fault and underlying mylonite zone. Leucogranite mylonites interlayered and dispersed within the quartzite and carbonate mylonites were also sampled from various depths. Quartz, feldspar, biotite, and whole rock samples from the silicate rocks, and calcite from the carbonate rocks were analyzed. In addition to the Secret Creek locality, other samples from similar structural levels close to the detachment fault were taken from the silicified breccia outcrops at Wilson Creek and near the Harrison Pass pluton (Fig. 1). In addition, a veined Permian limestone overlying the Diamond Peak Formation ~0.5 km north of Secret Creek gorge was also sampled.

Hydrogen isotope analyses were also made of a number of samples from the Northern Ruby Mountains (both near Tertiary normal faults and at lower structural depth), including biotite from pelitic schist mylonites at Secret Creek gorge itself. The data are given in Table 3 along with locality and petrographic information.

Table 1. Oxygen isotope compositions of silicate whole rocks and mineral separates from Secret Creek Gorge, Nevada

Sample	Rock-type	Material analyzed	$\delta^{18}O$	Location	Depth below contact with Horse Creek unit (meters)
Quartzite-schist (all mylonitic)					
HFSP 70	Quartzite	W.R.	+4.0	Transect A	−20.0
HFSP 153	Quartzite	W.R.	+7.7	Transect B	−48.5
HFSP 64	Quartzite	W.R.	+11.0	Transect A	−36.0
HFSP 68	Pelitic schist	W.R.	−0.1	Transect A	−20.5
		biotite	−0.4		
HFSP 77	Quartzite	W.R.	+2.8	Transect A	−7.5
		quartz	+3.1		
HFSP 78	Pelitic schist	W.R.	+0.7	Transect A	−7.5
HFSP 152	Pelitic schist	W.R.	+10.7	Transect B	−46.0
HFSP 16	Quartzite	W.R.	+11.6	Transect B	−37.0
HFSP 47	Quartzite	W.R.	+7.3	Transect B	−10.5
HFSP 49	Quartzite	W.R.	+7.0	Transect B	−10.0
HFSP 149	Quartzite	quartz	+9.8	Transect B	−41.0
H-15	Quartzite	W.R.	+10.5	Transect A	−35.0
H-17	Quartzite	W.R.	+8.0	Transect A	−31.5
H-26A	Quartzite	W.R.	+10.9	Transect A	−39.5
H-26B	Quartzite	W.R.	+11.1	Transect A	−39.5
H-8	Quartzite	W.R.	+3.6	Transect A	−7.0
H-11	Quartzite	W.R.	+6.3	Transect A	−11.0
H-12	Quartzite	W.R.	+5.5	Transect A	−9.5
H-22	Quartzite	W.R.	+9.0	Transect A	−10.0
H-23	Quartzite	W.R.	+11.0	Transect A	−21.0
H-24	Quartzite	W.R.	+10.7	Transect A	−20.5
HFSP 148	Pelitic schist	Biotite	+4.2	Transect B	−40.5
HFSP 150	Pelitic schist	Biotite	+5.8	Transect B	−45.0
Leucogranites (within quartzite-schist)					
HFSP 23	Leucogranite	W.R.	+6.3	Transect B	−40.0
		Quartz	+9.6		
		Feldspar	+5.1		
HFSP 65	Leucogranite	W.R.	+5.8	Transect A	−35.0
		Quartz	+8.8		
		Feldspar	+4.0		
HFSP 75	Leucogranite	W.R.	+4.3	Transect A	−7.5
		Quartz	+6.5		
		Feldspar	+5.4		
HFSP 67	Leucogranite	Quartz	+9.3	Transect A	−25.5
		Feldspar	+3.5		
HFSP 20	Leucogranite	Quartz	+10.9	Transect B	−41.5
		Feldspar	+7.7		
HFSP 147	Leucogranite	Quartz	+11.5	Transect B	−38.0
		Feldspar	+8.0		
HFSP 143	Leucogranite	Quartz	+10.9	Transect B	−10.0
		Feldspar	+7.3		
HFSP 144	Leucogranite	Quartz	+11.2	Transect B	−20.5
		Feldspar	+6.6		
		Biotite	+5.8		
Leucogranites (within Horse Creek assemblage)					
HFSP 89	Leucogranite	Quartz	+11.7	Transect A	–
		Feldspar	+4.0		
HFSP 138	Leucogranite	Quartz	+15.4	Transect B	–
		Feldspar	+11.3		
HFSP 57	Leucogranite	Quartz	+15.0	Transect A	–
		Feldspar	+13.9		
HFSP 92	Leucogranite	Quartz	+14.9	Transect A	–
		Feldspar	+7.0		

Table 1 (continued)

Sample	Rock-type	Material analyzed	$\delta^{18}O$	Location	Depth below contact with Horse Creek unit (meters)
Silicified breccias					
HFHP 3	Silicified breccia	W.R.	+0.1	Harrison Pass	–
HFHP 5	Silicified breccia	W.R.	−4.4	Harrison Pass	–
HF-N	Silicified breccia	W.R.	+4.0	Wilson Creek	–
HF-O	Silicified breccia	W.R.	+7.0	Wilson Creek	–
Horse Creek assemblage (silicates)					
HFSP 80	Vein quartz	W.R.	+14.2	Transect A	–
HFSP 137	Calc-schist	W.R.	+9.3	Transect B	–
		biotite	+6.3		
		vein calcite	+5.2 ($\delta^{13}C = -4.2$)		

Table 2. Oxygen and carbon isotope compositions of calcite and quartz from carbonate rocks at Secret Creek gorge, Nevada

Sample	Rock-type	Material analyzed	$\delta^{18}O$	Location	$\delta^{13}C$	wt% $CaCO_3$
Carbonate rocks[a] (Horse Creek assemblage)						
HFSP 135	Carbonate mylonite	Matrix	+14.2	Transect B	−3.6	
		Vein quartz	+12.5			
HFSP 133	Carbonate mylonite	Matrix	+19.6	Transect B	0.0	
		Vein calcite	+17.9		−0.1	
HFSP 132	Carbonate mylonite	W.R.	+20.8	Transect B	−0.3	
HFSP 139	Carbonate mylonite	W.R.	+17.5	Transect B	−0.8	
HFSP 131	Carbonate mylonite	W.R.	+15.3	Transect B	−4.2	
HFSP 55	Carbonate mylonite	W.R.	+20.3	Transect A	−0.6	
HFSP 90	Carbonate mylonite	W.R.	+15.7	Transect A	−0.1	
HFSP 140	Carbonate mylonite	W.R.	+14.5	Transect B	−1.5	
Metadolomite (Snoke and Howard 1984)						
HFSP 127	Dolomitic limestone	Matrix	+4.1	Transect C	−1.0	
		Vein quartz	+5.1			
Guilmette formation						
HFSP 118	Limestone	W.R.	+5.7	Transect C	+2.3	90
HFSP 122	Limestone	Matrix	+11.5	Transect C	+0.9	73
		Vein calcite	+0.8		+0.7	100
HFSP 119	Limestone	Vein calcite	−0.8	Transect C	+1.1	100
Upper plate limestone						
HF-J		Matrix	+17.8	Transect C	−0.8	84
		Vein calcite	+7.2		+0.2	80
HF-B		W.R.	+12.7	Transect C	−1.2	83
HF-A		W.R.	+22.8	Transect C	+3.3	90
HF-10		W.R.	+21.9	Transect C	−1.4	69

[a] All analyses calcite unless otherwise indicated

Stable isotope analyses

Oxygen was extracted from the silicates using a fluorination technique similar to that described by Taylor and Epstein (1962). Samples comprised either whole-rock powders or mineral separates. CO_2 from the carbonate samples was extracted using the H_3PO_4 method of McCrea (1950). The calcite data were corrected using the fractionation factor 1.01020 (modified from Sharma and Clayton (1965) by Friedman and O'Neil (1977)). The oxygen isotope data are reported in the δ-notation relative to Standard Mean Ocean Water (SMOW). The NBS 28 quartz standard has a value of +9.6 on this scale.

Hydrogen isotope data for hydrous minerals and fluid inclusions were obtained using the method of Vennemann and O'Neil (1991). Samples of approximately 20 milligrams are weighed into VYCOR tubes, covered with decrepitated quartz crystals, and are degassed at 150° C. They are then heated to 1400° C and the liberated gases passed over a CuO furnace held at 600° C. Water is collected and purified cryogenically and then transferred to a pyrex tube containing zinc. This tube is sealed under vacuum and the zinc and water reacted at 500° C for 20 min. The hydrogen produced by this reaction is introduced into the mass spectrometer where its amount and isotopic composition are determined. The precision of δD values and yields for the samples analyzed in this

Table 3. Hydrogen and oxygen isotope values of minerals and a fluid inclusion from Secret Creek Gorge and the Northern Ruby Mountains, Nevada

Sample	Rock-type	Mineral	δD	$\delta^{18}O$
RB-62[b]	Quartzite mylonite	Muscovite	−115	+9.0
		Biotite	−128	+5.0
HFSP 144	Pelitic schist mylonite	Biotite	−157	+5.8
HFSP 137	Pelitic schist mylonite	Biotite	−147	+6.3
HFSP 148	Pelitic schist mylonite	Biotite	−155	+4.2
HFSP 68	Pelitic schist mylonite	Biotite	−152	−0.4
Lam Can[a]	Granite gneiss	Biotite	−97	+7.7
RM-3-66[a]	Granite gneiss	Muscovite	−84	+9.8
		Biotite	−150	+7.0
J4b[a]	Granite (Jurassic)	Muscovite	−58	+9.1
RM-17-66[a]	Granite (Cretaceous)	Muscovite	−62	+11.5
		Biotite	−103	+9.6
RM-2-72[a]	Amphibolite	Hornblende	−145	+12.0
		Biotite	−148	+9.0
RM-20-68[a]	Mica schist	Muscovite	−47	+7.6
		Biotite	−97	+5.2
RM-26-68[a]	Quartzite	Hornblende	−172	+8.0
		Biotite	−155	+5.4
RM-28-68[a]	Schist	Hornblende	−174	+9.7
		Biotite	−155	+0.6
RM-49-68[a]	Biotite schist	Biotite	−134	+7.0
RM-50-68[a]	Gneiss	Biotite	−175	+0.0
RM-56-68[a]	Quartzite	Muscovite	−55	+10.4
		Biotite	−90	+7.7
RM-39-68[a]	Silicified breccia	Quartz	–	−4.9
		Inclusion water	−119	–

[a] The $\delta^{18}O$ values and sample locations of these samples are published in Kistler et al. (1981)
[b] Also published in Wickham et al. (1991)

study are ±2 and ±0.01 weight percent, respectively. The δD value of NBS-30 biotite is −65 at the University of Michigan.

Stable isotope data

Previous isotopic data

The first oxygen isotope data from the Northern Ruby Mountains were reported by Kistler et al. (1981), and included analyses of samples of mica schist, quartzite and gneiss. Some of these samples had unusually low $\delta^{18}O$ values for metasediments (e.g. quartz from a mica schist had $\delta^{18}O = +8.1$). More recently, similar low values in high-grade mica schists were reported from the Lizzies Basin locality in the East Humboldt Range (see Fig. 1; Wickham and Peters 1990). The values reported by Kistler et al. (1981) and Wickham and Peters (1990) were not sufficiently low to *require* meteoric water to have interacted with any of the rocks analyzed. This is not true of subsequent data from the Secret Creek area. Wickham et al. (1987, 1991) analyzed fifteen samples of whole-rock and mineral separates from this area and found very low $\delta^{18}O$ values in calcite veins ($\delta^{18}O \sim +1$) and evidence of isotopic disequilibrium between quartz and feldspar in leucogranite mylonite. Particularly noteworthy is the leucogranite mylonite sample RB 59, in which the quartz has a 'normal' $\delta^{18}O$ of +10.9, while the whole-rock value is +3.1. Inasmuch as the rock comprises mostly quartz and feldspar, these data indicate a low, probably negative, $\delta^{18}O$ value for the feldspar. Although $\delta^{18}O$ values of quartz, biotite and muscovite in the quartzite mylonite sample RB62 are similar to the values observed in quartzites from deeper structural levels (Wickham and Peters 1990), δD is anomalously low in the two mica samples. The extremely ^{18}O- and D-poor samples must have exchanged with a low-^{18}O fluid, and suggest that local meteoric water has interacted with the Secret Creek mylonite zone. These preliminary data provided the impetus for a more detailed stable isotope study of the Secret Creek area.

Footwall quartzite mylonites

The $\delta^{18}O$ value of each quartzite sample is plotted in Fig. 6, which relates each sample to depth below the low angle fault separating the quartzite-schist unit from the Horse Creek assemblage. Some of the quartzite mylonites have very low $\delta^{18}O$ values relative to those of structurally lower unmylonitized quartzites in the Ruby Mountains (Kistler et al. 1981), at Lizzies Basin (Wickham and Peters 1990) and elsewhere in the East Humboldt Range (Wickham et al. 1991; see Fig. 7). The $\delta^{18}O$ values of quartzite mylonite range from +11.6 to +2.8 (all samples containing ≥95% modal quartz) with a mean of +7.6. Nine of the nineteen samples have $\delta^{18}O < +8$. These values are significantly lower than those of unmylonitized quartzites from Lizzies Basin (see Figs. 1 and 7), most of which are between +10 and +12 (Wickham and Peters 1990). The quartzites from both localities are compositionally very similar and the

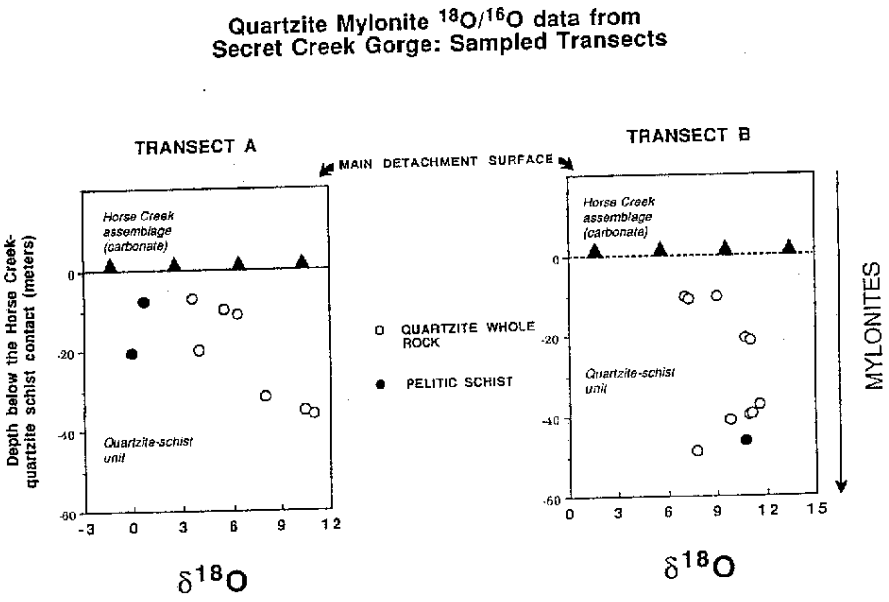

Fig. 6. Quartzite and pelitic schist mylonite whole-rock data plotted against depth within the quartzite-schist unit relative to the Horse Creek contact (see Fig. 3 for transect location, Fig. 8 for Horse Creek carbonate data). For transect B this contact is obscured by talus and its approximate location is shown by a dashed line. Note the extremely low $\delta^{18}O$ values of some of the quartzites (which are $\geq 95\%$ modal quartz), implying that there was exchange between these mylonites and low-^{18}O fluids (see text)

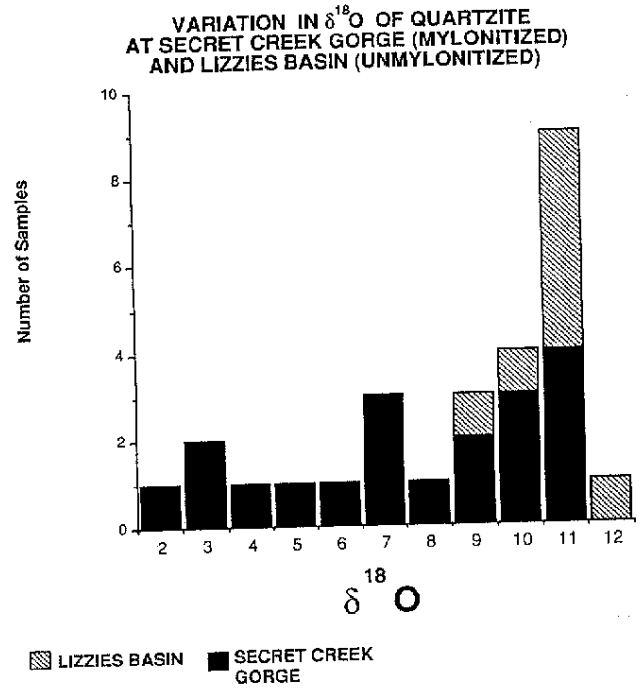

Fig. 7. Histogram of whole-rock quartzite $\delta^{18}O$ values from Secret Creek gorge and Lizzies Basin in the East Humboldt Range (see Fig. 1 for location)

contrast in $\delta^{18}O$ indicates that significant ^{18}O-depletion has occurred in the Secret Creek mylonites, even in quartz, a mineral that is quite resistant to oxygen isotope exchange with aqueous fluids (Gilletti and Yund 1984; see below). Figure 6 includes data for three pelitic schist mylonites, two of which have $\delta^{18}O$ values that are lower than those of any of the quartzite samples.

The $\delta^{18}O$ values of the quartzite-schist mylonites range widely, indicating that on a scale of tens of meters, isotopic alteration of quartz was not uniform. Large variations of the order of several per mil occur within Transect A over only 2–3 meters depth range and the variations along strike are even more extreme (compare Transects A and B, Fig. 6). In fact, there is a weak negative correlation in Transect A between structural depth and ^{18}O-depletion with the smallest isotopic shifts occurring in the three deepest samples. There is no such correlation in the data of Transect B. The reasons for this variation in the degree of ^{18}O-depletion in quartz are unresolved at this point, but it may be related to the mechanism and timing of fluid infiltration (see below).

The depth range over which extreme ^{18}O-depletion occurs is significant. A quartzite mylonite sample from 7.5 m below the low angle fault at the top of the quartzite-schist unit has a $\delta^{18}O$ of $+2.8$, and an adjacent pelitic mylonite has a $\delta^{18}O$ value of $+0.7$. At 20.5 m depth a quartzite has a value of $+4.0$, and an adjacent mica-rich quartzite has a value of -0.1. These rocks are approximately 21 and 34 m, respectively, below the main detachment fault that is the upper limit of the mylonite zone (see Fig. 4). The ^{18}O-depletion is therefore *not* restricted to the brittley deformed upper plate rocks, but is manifest at least several tens of meters into the lower plate quartzite mylonites. In general, more feldspathic and micaceous metasediments are slightly more ^{18}O-depleted than pure quartzites from the same structural level, although this may be simply a reflection of changes in the modal amounts of feldspar and mica. Note that the lowest quartzite samples in both Transect A and B are significantly more ^{18}O-depleted than typical unmylonitic quartzite from deeper levels in the lower plate rocks. It is therefore clear that significant isotopic alteration occurred at the depth of the deepest exposures accessible at Secret Creek (~ 50 m into the quartzite-schist) and that low-^{18}O fluids were able to penetrate *at least* 70 m below the detachment fault at this location.

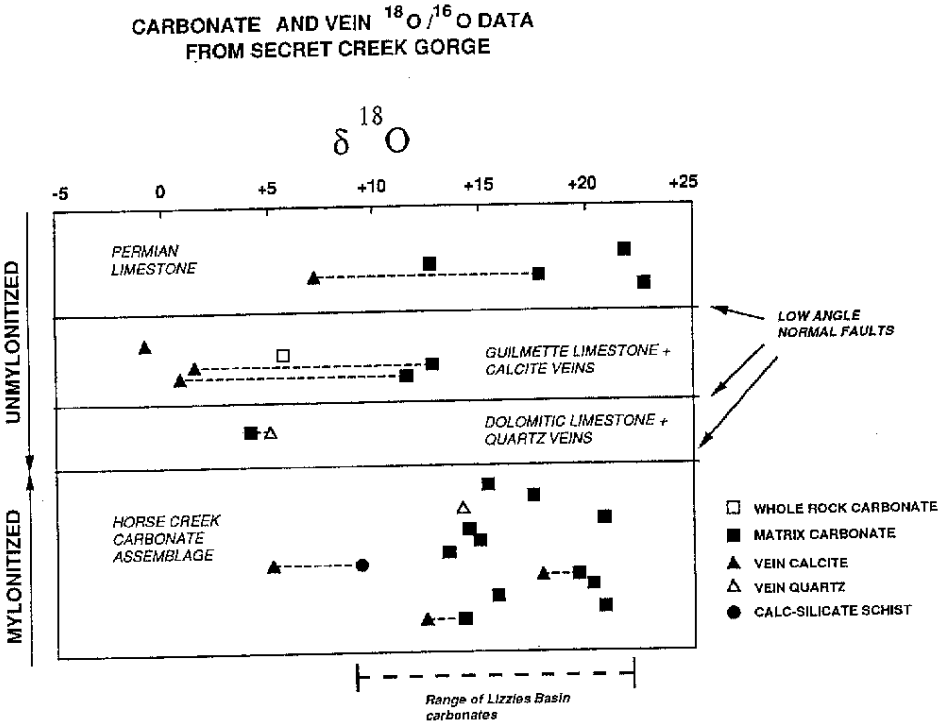

Fig. 8. Calcite $\delta^{18}O$ values from both the Horse Creek mylonite assemblage and the overlying unmylonitized carbonate fault slices plotted according to their relative structural position in the Secret Creek gorge area. The matrix Horse Creek marble values fall in the same range as structurally lower unmylonitic marbles from Lizzies Basin. Veins are intensely folded in this unit and have similar $\delta^{18}O$ values as the matrix calcite, possibly reflecting post-infiltration reequilibration with ^{18}O-rich carbonate. Within most of the structurally higher unmylonitic units the matrix carbonate $\delta^{18}O$ values are normal for the upper plate (see text), but quartz, and especially calcite veins are much lower, in one case negative. This diagram represents a structural thickness of about 45 m

Secret Creek carbonate rocks

^{18}O-depletion is also observed in the (amphibolite facies) carbonate mylonite and in the (low-grade) upper plate carbonates, but in general the effects are much more extreme in vein material. The carbonate matrix has a more uniform, moderately ^{18}O-depleted isotopic composition.

Horse Creek assemblage. Calcite analyzed from unveined parts of mylonitized Horse Creek marbles has $\delta^{18}O$ values in the range +20.8 to 14.2, depending on position in the section (Fig. 8). Vein quartz and calcite within the carbonate mylonite usually has a slightly lower $\delta^{18}O$ value than adjacent matrix material, although a calcite vein in one of the calc-silicate schist boudins has a much lower $\delta^{18}O$ value of +5.2, similar to those of veins in the upper plate rocks. The carbonate mylonites at Secret Creek have the same wide range of values observed in *unmylonitized* amphibolite facies marbles from deeper structural levels, such as at Lizzies Basin, where the range is +9 to +22 (Wickham and Peters 1990). The Lizzies Basin systematics have been ascribed to exchange with deep-seated metamorphic and igneous pore fluids (Wickham and Peters 1990), and the Horse Creek marbles could have inherited similar systematics from their earlier metamorphic history.

Dolomitic limestone. This low-grade unmylonitized carbonate is pervasively veined by quartz; the matrix calcite has a $\delta^{18}O$ value of +5.1, and the quartz a value of +4.1. This is the only upper plate unit sampled that had a matrix calcite value below +11.5, possibly resulting from exchange between low-^{18}O fluids and the matrix calcite as the unit was infiltrated on the μm scale.

Upper Plate limestone and other carbonate rocks. The rest of the overlying low-grade unmylonitized veined carbonate fault slices at Secret Creek and the Permian limestone have $\delta^{18}O$ values of matrix calcite that range from +22.8 to +11.5 (Fig. 8). This overlaps the range of the structurally higher, upper-plate unmylonitized carbonates in the Ruby-East Humboldt Range, whose values range from +12.8 to +18.5 (Wickham et al. 1987, 1991). These relatively high matrix $\delta^{18}O$ values are in direct contrast to those of the veins within the calcite matrix. The calcite veins in the Guilmette fault slice have values ranging from +0.8 to +1.5, while two samples of the carbonate matrix have $\delta^{18}O$ values of +11.5 and +12.8. In general $\delta^{18}O$ values of the calcite veins are 10 per mil lower than those of the matrix carbonate (Fig. 8). Wickham et al. (1991) relate the upper plate limestone $^{18}O/^{16}O$ systematics in the Southern Ruby and Egan Ranges to variable interaction with low temperature, probably surface derived, fluids during the

Cenozoic and this may also explain the upper plate matrix values at Secret Creek. It is not certain that this occurred during the same meteoric fluid infiltration event documented by the vein material. The $\delta^{13}C$ values of all the samples are fairly constant, mostly varying from -0.8 to $+1.5$ and probably represent depositional (sedimentary) values.

Footwall leucogranite mylonites

As noted above, these rocks were less extensively mylonitized than the metasedimentary rocks that they intrude, and often consist of large feldspar porphyroclasts within a finer, dynamically recrystallized quartz matrix. $\delta^{18}O$ values of quartz and feldspar from these rocks are plotted in relation to depth in the Secret Creek section in Fig. 9. There is pronounced oxygen isotope disequilibrium in most samples, confirming the tentative conclusions drawn from the preliminary quartz and whole-rock data of Wickham et al. (1991). A wide range of fractionations is observed (see below), but in general the leucogranites intruding the quartzite-schist unit have been more strongly ^{18}O-depleted than those intruding carbonates. As with the quartzites, however, the depletion is quite heterogeneous on a scale of meters. In the Horse Creek assemblage there are large disequilibrium effects in some leucogranites, while others preserve normal igneous values similar to those reported by Kistler et al. (1981) from elsewhere in the Northern Ruby Mountains.

Figure 10 clearly illustrates any departure from equilibrium in quartz-feldspar pairs, evidenced by the large positive slope of the array of points, most of which plot well below the $\Delta = 1$ and 2 per mil lines. These lines correspond to typical igneous fractionations at temperatures of $\sim 800°$ C and $\sim 500°$ C respectively (Clayton et al. 1989; Chiba et al. 1989), fractionations that are also typical of other unmylonitized igneous rocks in the Ruby Mountains (Kistler et al. 1981). Such steep disequilibrium quartz-feldspar arrays are typical of the systematics observed in shallowly emplaced plutons that have interacted with meteoric-hydrothermal systems, and are sensitive indicators of the extent of meteoric-hydrothermal infiltration that has occurred (Gregory et al. 1989; see below).

Fault breccias and breccia sheets

The Wilson Creek silicified fault breccia has low $\delta^{18}O$ values of $+4.1$ and $+7.0$, which indicate interaction with a low-^{18}O fluid, probably the same fluid that was responsible for deposition of the siliceous breccia matrix. Two samples from the jasperoid breccia sheet overlying the Harrison Pass pluton (Fig. 1) have even lower values of $+0.1$ and -4.4. The latter sample (HFHP5) is an unstrained mass of white quartz several tens of meters thick, which probably precipitated directly from circulating hydrothermal fluid. This is one of the lowest $\delta^{18}O$ values of any sample that we have analyzed, and is consistent with the quartz precipitating from *pristine* local meteoric water ($\delta^{18}O \sim -16$) at a temperature of 200–250° C.

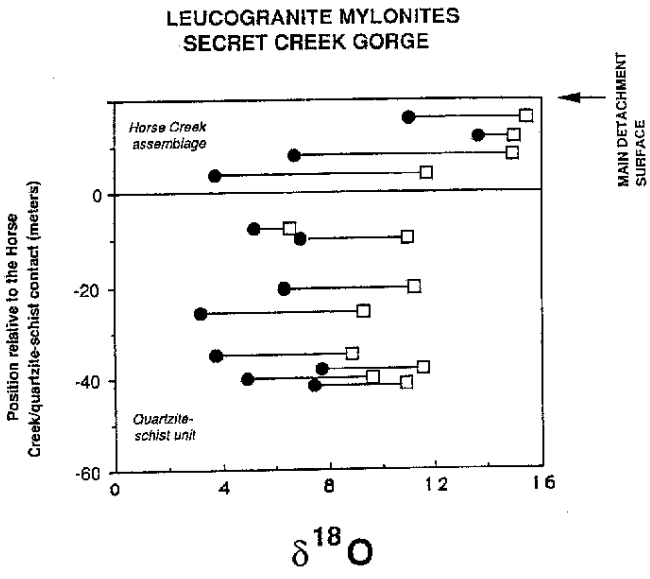

Fig. 9. $\delta^{18}O$ values for quartz and feldspar mineral separates from mylonitized leucogranite are plotted against structural position; (the diagram is a composite of samples from both transects A and B; see Figs. 3 and 7)

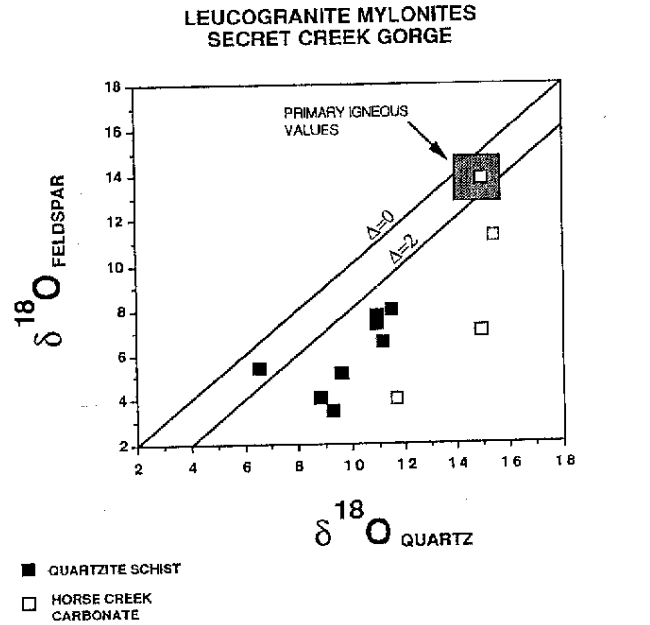

Fig. 10. $\delta^{18}O$ of quartz plotted against $\delta^{18}O$ of feldspar from mylonitized leucogranite at Secret Creek gorge. Equilibrium fractionation lines corresponding to $\Delta_{quartz\text{-}feldspar} = 0$ ($T \sim \geq 900°$ C) and $\Delta_{quartz\text{-}feldspar} = 2$ ($T \sim 500°$ C) are shown. Most of the data plot well below these lines, indicating isotopic disequilibrium between quartz and feldspar. All samples would probably have started close to the value of the most ^{18}O-rich Horse Creek data point ($\delta^{18}O_{quartz} = +15.0$; $\delta^{18}O_{feldspar} = 13.9$), which is similar to presumed undisturbed magmatic values recorded in leucogranites elsewhere in the northern Ruby Mountains (Kistler et al. 1981)

Hydrogen isotope data

The hydrogen isotope data (Table 3) provide additional evidence for the interaction of externally-derived fluid with the Secret Creek mylonites and other samples elsewhere in the Ruby Mountains. The δD values of pelitic schist mylonite biotites at Secret Creek are low and uniform, ranging from -147 to -157. Biotite from a quartzite mylonite has a δD value of -128. All of these values are much lower than those of biotite from the structurally lower Lizzies Basin locality, where the values of -58 to -68 lie within the range of typical plutonic igneous or metamorphic biotites. The Secret Creek biotites are mostly fresh and unchloritized and provide convincing evidence that low-D fluids penetrated and exchanged with most of the rocks in the Secret Creek area at moderately high temperatures. Because hydrogen is much more abundant in aqueous fluid than oxygen (relative to rocks), δD values are affected by small amounts of infiltration, much less than that required to shift δ^{18}O values (Taylor 1977). This explains the low, uniform δD value in the Secret Creek biotites and the much more variable δ^{18}O values.

Other samples from elsewhere in the northern Ruby Mountains have similar D/H systematics, although D-depletion is more heterogeneous. Samples located near Tertiary normal faults have very low δD values in comparison with those of structurally lower rocks (see Table 2 in Kistler et al. 1981 for exact locations). The D-depletion was widespread within the Ruby Mountains high-grade rocks, but only in the Secret Creek area are D- and ^{18}O-depletions coupled, presumably because it was only in this area that fluid/rock ratios were sufficiently high for this effect to be observed.

Discussion

Evidence for meteoric fluid infiltration and exchange

The mylonitized rocks at Secret Creek gorge must have exchanged with a very low-δ^{18}O fluid of meteoric origin. A quartz separate from HFSP 77 with a δ^{18}O value of $+3.1$ may be used to constrain the isotopic composition of the fluid. This sample would have been in equilibrium with a water of δ^{18}O $\sim +2$ at 650° C, or ~ -2 at 350° C (Clayton et al. 1972). The quartzite δ^{18}O values must therefore have been set by exchange with water of δ^{18}O $< +2$, and probably < 0 over the entire range of probable temperatures of interaction (see below). Meteoric water is the only major terrestrial reservoir of oxygen with the appropriate isotopic composition to be such a source (see, for example, Sheppard 1986). Although it is possible that quartz did not reach equilibrium with the infiltrating water (see below), this would imply an even lower value for water that exchanged with HFSP 77 because the quartz was shifted towards lower δ^{18}O values. This calculation, however, does provide a maximum estimate for the δ^{18}O of the water exchanging with quartz, and as such confirms meteoric water as the only possible exchanging fluid.

A good constraint on the composition of pristine Tertiary meteoric water at the time of detachment faulting in the northern Ruby Mountains is provided by a measurement of the hydrogen isotope composition of fluid inclusion water extracted from a sample of unstrained quartz in breccia sample RM-39-68 (collected by R. Kistler). This quartz has a very low δ^{18}O value of -4.9 and was obviously precipitated from water of meteoric origin. Using the δD-δ^{18}O relation of Craig (1961) and the measured δD value of -119, we calculate a δ^{18}O value of -16 for this inclusion fluid. This value is almost identical to that of modern and Tertiary meteoric water in this area (Sheppard et al. 1969) and in combination with the measured value for the quartz corresponds to a minimum formation temperature of about 240° C (Clayton et al. 1972; Matsuhisa et al. 1979), a plausible value for an upper plate rock.

Temperature of isotopic exchange

The temperature of exchange can be estimated by assuming a value for the isotopic composition of local meteoric water and then calculating a temperature range over which the samples equilibrated with this water. This treatment of the data for oxygen is complicated by the fact that it is not certain that the rocks equilibrated with pristine meteoric water, because such water could have been ^{18}O-shifted by exchange with other rocks as it flowed from the surface to the shear zone. In the case of quartz from the mylonites, it may also be unsound to use equilibrium isotopic fractionations to calculate temperatures or water compositions, because the quartz may not have fully equilibrated with the infiltrating fluid, or may have partly back-exchanged during waning of the hydrothermal system.

It is more reasonable to assume that the lowest δD values are close to equilibrium values because several samples have similar values, and because D/H ratios are much more sensitive to water infiltration than ^{18}O/^{16}O. It is also unlikely that D/H ratios have been reset at a late stage after mylonitization because most of the samples are fresh and unchloritized (O'Neil 1987). At Secret Creek gorge, the biotite samples have the lowest δD values (-157 to -147). These samples would be in equilibrium with the fluid inclusion water (RM-39-68) at a temperature of 480–620° C (Suzuoki and Epstein 1976), which provides a plausible estimate of the temperature of interaction. The δD values of samples from elsewhere in the northern Ruby Mountains, most of which are adjacent to normal faults, fall in a similar range (-160 to -175) and predict similar temperatures of equilibrium (although some of these were partly chloritized). These calculated temperatures are in close agreement with those estimated for mylonitization at Secret Creek and elsewhere in the East Humboldt Range by Hurlow et al. (1991), are consistent with the estimates of Hacker et al. (1990) and are similar to temperature estimates at other Cordilleran localities (Kerrich and Hyndman 1986; Smith et al. 1991).

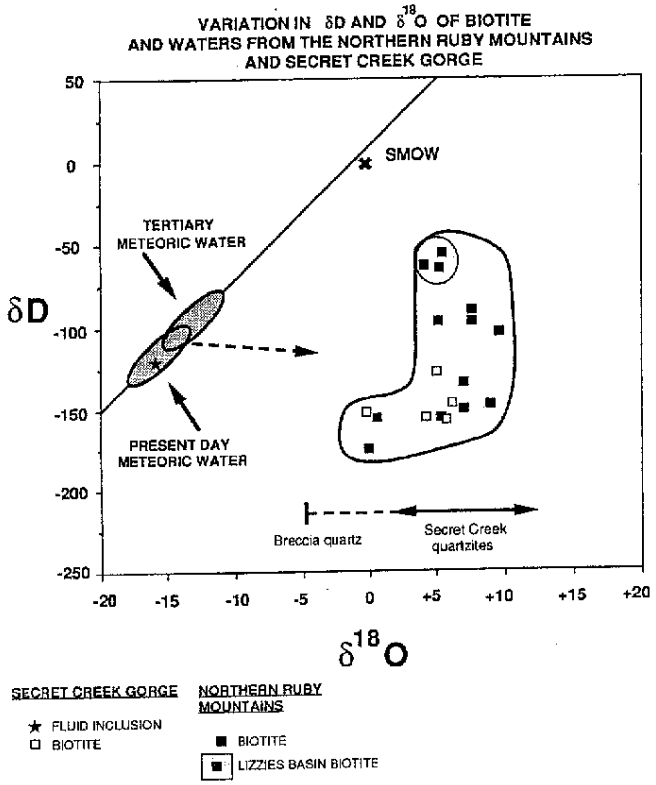

Fig. 11. The δD and $\delta^{18}O$ values of biotite from the northern Ruby Mountains and from Lizzies Basin in the East Humboldt Range (after Wickham et al. 1991). The meteoric water line and the field of northeastern Nevada waters during the Tertiary and at present (Sheppard et al. 1969; Sheppard 1986; O'Neil and Silberman 1974) are shown, together with the composition of the fluid inclusion water (RM-39-68) with a measured δD of -119 and calculated $\delta^{18}O$ of -16 (*star*). The data define a typical exchange trajectory ranging from pristine plutonic values (e.g., the Lizzies Basin biotites) to the most exchanged samples ($\delta^{18}O \sim 0$, $\delta D - 160$) which have had both their δD and their $\delta^{18}O$ values lowered by exchange with local meteoric water. These samples would have been in equilibrium with a water of $\delta^{18}O \sim +5$ and $\delta D \sim -120$ at a plausible exchange temperature of 500° C. Such a water could have evolved from local meteoric water along a path such as that shown by the *dashed line* and *arrow*

Isotopic evolution of the water

It is now possible to relate the estimated temperatures of exchange and the initial water composition in order to constrain the isotopic evolution of the meteoric water and the extent to which isotopic exchange occurred. These relations are illustrated in Fig. 11, where δD is plotted against $\delta^{18}O$ for all samples for which both were measured. Also shown is the meteoric water line with the field of waters from the Northern Great Basin in the Tertiary and at present-day from Sheppard et al. (1969) and Sheppard (1986). Tertiary meteoric waters from this region are estimated to have had $\delta^{18}O$ between -12 and -14 and δD between -90 and -110 based on analyses of supergene clays and other surficial materials (Sheppard et al. 1969) and fluid inclusions in meteoric-hydrothermal minerals (O'Neil and Silberman 1974). This compares with modern-day δD and $\delta^{18}O$ values of about -120 and -16. The position of the fluid inclusion water sample ($\delta D = -119$, $\delta^{18}O$ (calculated) $= -16$) is also plotted. The sample with the lowest δD value (-175) also has the lowest $\delta^{18}O$ value of any of the micas (0.0) and over this temperature range would have been in equilibrium with a water with $\delta^{18}O$ of $+4$ to $+6$ (Friedman and O'Neil 1977). These waters could have evolved from local meteoric waters which became progressively ^{18}O-enriched by exchange with the rocks through which they flowed, as indicated by the arrow in the diagram.

The biotite data from both Secret Creek gorge and elsewhere in the northern Ruby Mountains define part of a typical curved exchange trajectory on a δD-$\delta^{18}O$ plot. A field of data for pristine biotites from deep structural levels in the Ruby-East Humboldt Range (Lizzies Basin) is shown (Wickham et al. 1991), marking the likely initial compositions of the D- and ^{18}O-depleted biotites. Because the hydrogen content of biotite is small relative to its oxygen content, infiltration of isotopically light meteoric water will first change the δD values (at relatively low water-rock ratio) before it changes the $\delta^{18}O$ values (e.g. Taylor 1977).

The range of $\delta^{18}O$ of quartzite mylonites at Secret Creek, and the $\delta^{18}O$ of the breccia quartz that hosts the fluid inclusion sample are shown in Fig. 11. Note that the range for these samples is very similar to that of the mica and amphibole samples (see also Table 3), adding strength to our interpretation that all were isotopically altered by fluids of similar initial isotopic compositions. This is important because some of the D/H data are for samples from localities in the northern Ruby Mountains other than Secret Creek gorge, although many of these samples are close to major N-S trending Tertiary fault zones. The hydrogen isotope data suggest, therefore, that although Secret Creek is the only place where major ^{18}O-depletion of mylonites associated with abundant meteoric water infiltration is observed, smaller amounts of meteoric water (presumably associated with Tertiary normal faulting and breccia sheet formation) infiltrated over much wider areas.

An alternative way to analyze the data involves using transport theory to describe the propagation of isotopic anomalies by flow of fluid in a porous medium (e.g., Bickle and McKenzie 1987; Blattner and Lassey 1989). Figure 6 indicates that low $\delta^{18}O$ values extend at least 70 meters into the Secret Creek gorge mylonites (50 meters into the quartzite schist unit). The scatter in the data, and the suggestion in Transect A that the ^{18}O-depletion of the rocks decreases with depth, are consistent with the downward penetration of an oxygen isotope infiltration front that has become broadened by diffusive and dispersive processes. To a good approximation, such a front will travel at a velocity, W, given by the equation:

$$W \approx \frac{v_f \phi}{\left(\frac{\rho_s}{\rho_f} \cdot K_D\right)} \qquad (1)$$

where v_f is the fluid velocity, ϕ is the porosity, ρ_s and ρ_f the densities of solid and fluid respectively, and K_D

is the solid/fluid distribution coefficient (Bickle and McKenzie 1987). Although we do not have enough data to resolve it clearly (and are therefore unable to take account of diffusive or dispersive effects) if we assume that the front has moved approximately 70 m down from the detachment fault in 3×10^{13} s ($\sim$1 Ma, a time scale consistent with the isotopic disequilibrium arrays observed in leucogranite quartz-feldspar pairs and also with microstructural and geochronological studies – see section (6.7) below), then $W = 2.3 \times 10^{-12}$ m s^{-1}. Substituting appropriate values for ρ_s, ρ_f, and K_D into Eq. (1) and choosing a plausible porosity, ϕ, of 10^{-3} yields a value for v_f of 1.2×10^{-8}. The time integrated flux ($v_f \phi t$) may be estimated simply from the 70 meter minimum displacement distance to be at least $\sim 1.5 \times 10^2$ m^3/m^2. These are probably minimum values because the front may have penetrated further than 70 m into the lower plate. However, it is of interest to compare these estimates with the distance a hydrogen isotope front would travel for the same fluid velocity and time duration, which would be approximately 1500 m, assuming a rock H_2O content of $\sim$2 weight percent. The structurally deepest level at which anomalously low δD values have been found in the Ruby-East Humboldt Range is at Angel Lake, where two biotite samples have δD values of -88 and -108 (Wickham et al. 1991). All samples from below this level have normal "igneous" δD values of ~ -40 to -80. If Angel Lake corresponds approximately to the limit of penetration of the meteoric hydrogen infiltration front, then its structural depth of $\sim$1000–1500 m below the Secret Creek mylonites (A.W. Snoke, personal communication, 1991) is of the same order as the estimate made above, and is broadly consistent with downward penetrating "meteoric" hydrogen and oxygen infiltration fronts.

Comparisons between the upper and lower plates

In the upper plate rocks, subvertical quartz and calcite veins have some of the lowest δ^{18}O values of the entire data set (presumably because they were precipitated directly from relatively pristine meteoric water). The rock matrix, however, failed to exchange pervasively with these fluids as the δ^{18}O values are frequently $\sim$10 per mil higher (see Fig. 8). These data and the style of infiltration are in contrast to the data and observations from the lower plate mylonite zone. Here, clearly crosscutting veins are rare, rock textures are more homogeneous, and the low-^{18}O isotopic effects have been incorporated into the matrix quartz itself. Despite the absence of veins, there are many healed fractures (e.g. Fig. 5b), implying that these features were present earlier and were annealed and recrystallized by progressive mylonitization. Such cycling of brittle and ductile processes is believed to be a common feature of mylonite zones (Knipe 1989). This provides a clue to why the low-^{18}O signature has been incorporated into the quartzite mylonite matrix (rather than occurring in discrete low-^{18}O veins). Continual and repeated annealing and recrystallization of crosscutting, low-^{18}O quartz veins will promote oxygen isotope exchange and homogenization, both by enhancing exchange rates, and simply by converting vein material into matrix material during ductile flow (see below).

Isotopic exchange was evidently more effective within the quartzite schist and leucogranite mylonites than within the carbonate mylonites. Extremely low δ^{18}O values characteristic of meteoric fluids that are observed in the silicate mylonite lithologies do not occur within the Horse Creek marbles (Fig. 8) although the measured values ($+13$ to $+21$ for calcite in marbles) do not preclude small amounts of meteoric fluid infiltration. This may reflect the structural weakness and low permeability of the mylonitized carbonates relative to the mylonitized quartzites. The stronger quartzites were able to support larger deviatoric stresses leading to the formation of transient downward penetrating fractures that could convey upper plate fluids a short distance into lower plate rocks. The weaker marble mylonites could sustain only low deviatoric stresses, showed a lesser tendency to fracture, and consequently remained relatively impermeable to the infiltrating fluids. Upper plate rocks were strongly veined but much less pervasively exchanged. The isotopic compositions of veins suggest that fluids had more pristine δ^{18}O values and fluid-rock interaction probably ranged to lower temperatures.

Evidence for fluid infiltration during mylonitization

The spatial coincidence of the low-^{18}O rocks at Secret Creek with the mylonites suggests that mylonitization and ^{18}O-depletion may be linked. This idea gains further support from the temperature estimates based on exchange of hydrogen isotopes between local meteoric (and fluid inclusion) water and mylonite biotite, which are similar to those made by Hurlow et al. (1991) and Hacker et al. (1990) of the temperature of mylonitization ($\sim$400–620° C). The occurrence of annealed veins within the mylonites and the rarity of post-mylonitization veining or fracturing also suggests that water infiltration accompanied mylonitization. Experimental studies of natural quartz lend further strong support to this hypothesis by suggesting that the $\sim$10 per mil shifts observed in some quartzite mylonites could not have occurred at low temperatures. Giletti and Yund (1984) demonstrated that quartz is very resistant to diffusive oxygen isotope exchange with water at temperatures below 450° C. The large observed isotopic shifts could only have occurred at higher temperatures (or during dynamic recrystallization – see below). The experimental quartz-water exchange data exclude any possibility that the large isotopic shifts found in some of the quartzite mylonites (Figs. 6 and 7), where we are certain that ^{18}O-depletion affected the quartz itself, are a post-mylonite, low-temperature effect. The isotopic exchange process must have occurred prior to or concurrently with mylonitization.

It has been suggested that plastic deformation (i.e. mineral recrystallization) greatly enhances the rate of oxygen isotope exchange between water and quartz (Giletti 1985; Sharp et al. 1988), thereby allowing substantial isotopic alteration to occur at temperatures where exchange between this mineral and aqueous fluids is normally sluggish. The lower temperature limit of this type

of behavior is not well constrained because the exact temperature at which plastic deformation is replaced by brittle fracturing is not well known and depends on a variety of other factors. In the case of the Secret Creek gorge mylonites, these observations simply imply that infiltration and exchange were most likely confined to the mylonitization event itself.

Discrete, crosscutting, undeformed (post-mylonitization) veins are very rare in the quartzite mylonites, and there is no tendency for the low-^{18}O values to be associated with these features. The combined isotopic and petrographic data are compatible with the lower plate rocks being infiltrated by a variably ^{18}O-shifted meteoric water with $\delta^{18}O$ of -5 to 0 and δD of -110 to -130 (close to its original value) during mylonitization at temperatures of 400°–620° C. Transient fracturing events generated veins which were subsequently deformed with this material then incorporated into the quartzite matrix. Oxygen isotope exchange was probably facilitated by infiltration occurring synchronous with mylonitization, but otherwise would have required high temperatures (>400° C) similar to the estimated conditions of mylonitization. Since meteoric fluids at Secret Creek probably interacted with rock at temperatures >400° C, they must have penetrated *at least* 5 km below the surface. Because Hurlow et al. (1991) estimate pressures of mylonitization between 3 and 4 kbars, it is possible that the surface fluids penetrated to depths in excess of 10 km.

Infiltration mechanisms

Reynolds and Lister (1987) have discussed rock mechanical constraints on fluid movement in the vicinity of detachment faults. They suggested that in extensional environments where σ_1 (the greatest principal compressive stress) is vertical, upperplate fluids will in general be at or close to hydrostatic pressure and will occupy subvertical fracture zones penetrating from the surface to the vicinity of the detachment fault. Upper plate fluids will be dominated by ground water from meteoric or connate sources. This model explains very well both the orientation of upper plate fractures and the isotopic composition of vein fillings in the Ruby-East Humboldt Range upper plate rocks. Vigorous circulation of meteoric fluids through the fracture systems, driven by the rapid uplift of anomalously warm lower plate rocks, could have promoted deposition of the vein material and also caused the intense silicification noted within some of the upper plate breccias (e.g. the Wilson Creek breccia).

Within the lower plate rocks below the detachment fault, Reynolds and Lister (1987) proposed that fluid pressure is much higher, close to lithostatic, and locally exceeds σ_3, generating transient fractures and veins (also usually steeply dipping) that become overprinted by mylonite fabrics. They proposed that these lower plate rocks should be dominated by deep-seated fluids derived from deeper level igneous or metamorphic sources, and that there should be only one-way connection between the upper and lower plates with fluids mainly expelled upwards. This view of mylonite zones as lithostatically pressured impermeable boundaries has also been proposed by Kerrich and Hyndman (1986) and Kerrich and Rehrig (1987). These models of lower-plate fluid flow are supported by the stable isotope data of Smith et al. (1991) for the South Mountains detachment fault zone in Arizona. They found no isotopic evidence for infiltration of surface fluids into the lower plate mylonites and observed virtually no change in the $\delta^{18}O$ and δD values of mylonite lithologies compared with their unmylonitized protoliths. They concluded that the fluids which interacted with the mylonites were derived from a local deep-seated igneous source, namely local Tertiary granitoid intrusives.

The oxygen isotope analyses of the Secret Creek lower plate mylonites are in striking contrast to the data from the South Mountains, or indeed from most other Cordilleran detachment fault zones for which stable isotope data have been published. They provide direct evidence that meteoric fluids may indeed penetrate across the brittle-ductile transition into lower plate, plastically deforming rocks (as discussed in section 6.5). This evidence contradicts the view of Reynolds and Lister (1987) that surface-derived fluids are restricted to the upper plate (although these authors admitted the possibility that "dilatancy pumping and ... convection could draw upper plate fluids into the brittle segments of the detachment zone"). It is, however, consistent with the interpretation of Kerrich (1988) that meteoric water penetrated mylonites in the Buckskin Range, Arizona to depths in excess of 15 km, based on a single δD value of -127 in a chlorite-biotite mixture separated from a mylonite.

Dilatancy (or seismic) pumping is the most plausible mechanism by which upper plate (hydrostatically pressured) fluid can penetrate into the lower plate mylonites. Such a mechanism has been proposed by several workers (e.g., Sibson et al. 1975; Sibson 1983; Etheridge et al. 1983, 1984; McCaig 1984, 1988) and occurs when fault zone rocks draw adjacent fluid into them due to dilatancy induced by microcracking during the buildup of stress prior to failure. In this way rocks at deeper levels (e.g. the lower plate mylonites) can develop underpressured extensional fractures and draw down pore fluids from higher structural levels. This could have occurred during exhumation of the lower-plate rocks, when brittle fracture and plastic flow were both occurring contemporaneously within the mylonite zone, as strain became isolated along certain planes or zones (Hacker et al. 1990). At this time, meteoric water in the upper plate rocks at Secret Creek could have been drawn down into the mylonite zone along extensional fractures. The resulting macroscopic veins were continuously annealed away during subsequent plastic flow, although their textural remnants can be clearly seen within the quartzite mylonites (see Fig. 5b).

Duration of fluid flow

Microstructural studies of the mylonites at Secret Creek gorge suggest strain rates of 10^{-11} to 10^{-12} s^{-1}, corre-

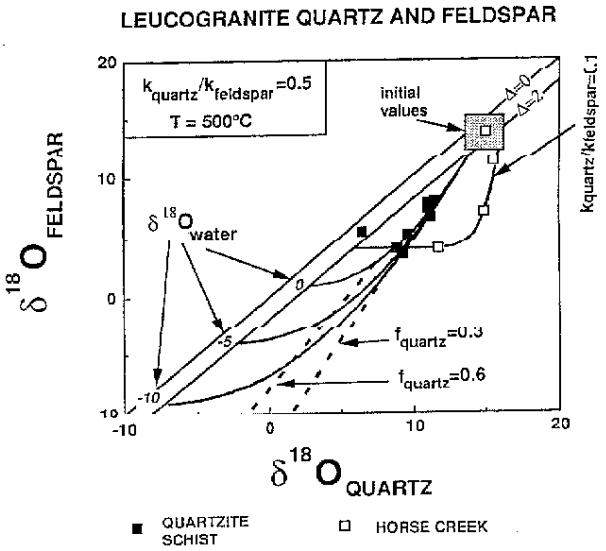

Fig. 12. $\delta^{18}O_{quartz}$ and $\delta^{18}O_{feldspar}$ for leucogranite mylonite samples within the Horse Creek assemblage and quartzite schist unit (compare with Fig. 11) with calculated exchange trajectories (see Gregory et al. 1989). The quartzite-schist leucogranite array is approximated by trajectories in which the kinetic rate constant of feldspar ($k_{feldspar}$) is twice that of quartz. These trajectories start from the point $\delta^{18}O_{quartz}=+14$, $\delta^{18}O_{feldspar}=+12$ and end at points in equilibrium with waters with $\delta^{18}O=0$, -5, and -10 assuming that $\Delta_{quartz\text{-}water}=3$ and $\Delta_{feldspar\text{-}water}=2$ (which corresponds to a temperature of ~500° C). The dashed lines are isochrons of constant $f_{quartz}=0.3$ and 0.6, the former value closely approximating the slope of the quartzite-schist array. The distinctly different Horse Creek array is steeper and requires a lower value of $k_{quartz}/k_{feldspar}$. In this case a single trajectory for $k_{quartz}/k_{feldspar}=0.1$ is shown starting from $\delta^{18}O_{quartz}=+16$, $\delta^{18}O_{feldspar}=+14$ and finishing in equilibrium with a water of $\delta^{18}O=+3$. See text for further details

sponding to uplift rates of ~6 km/Ma (Hacker et al. 1990). They estimate that for a plausible shear zone geometry, movement on the shear zone at this strain rate could have lasted 2–3 Ma. This compares with constraints from ^{40}Ar-^{39}Ar ages that suggest cooling over an extended period from 500° C at ~45 Ma to 300° C at ~22 Ma (Dallmeyer et al. 1986).

Stable isotope analysis of quartz and feldspar from leucogranite pods within quartzite and carbonate mylonites at Secret Creek gorge can also be used to constrain the duration of hydrothermal interaction. The $\delta^{18}O$ values of quartz and feldspar mineral separates are plotted in Figs. 10 and 12. Although some samples have typical high-temperature $\Delta_{quartz\text{-}feldspar}$ of 1 to 2 per mil, most of the data form a steep array of points that are clearly distinct from the equilibrium 45° line, indicating open system equilibration with infiltrating meteoric fluid (Gregory et al. 1989). Moreover, the data for leucogranites within the carbonate mylonites of the Horse Creek assemblage define a distinctly different, steeper, trajectory than those within the quartzite schist, suggesting differences in the infiltration and exchange history of granites in the two units. These types of steep arrays are commonly observed in meteoric hydrothermal systems associated with high-level granitic plutons (Gregory and Criss 1986; Criss and Taylor 1986) and result from water exchanging more rapidly with feldspar than with quartz.

Criss et al. (1987) and Gregory et al. (1989) present a detailed analysis of oxygen isotope exchange kinetics among mineral pairs with contrasting exchange rates. The calculated trajectories for exchange between minerals and water of various isotopic compositions (given by Eq. (15) of Gregory et al. 1989) may be used to construct isochrons that represent lines of constant f or fraction of exchange. These may be directly transformed into the dimensionless parameter kt where k is a kinetic rate constant and t is the time elapsed, using the equation $\ln(1-f)=-kt$ (Eq. (14) of Gregory et al. 1989). Some theoretical exchange trajectories for a fluid-dominated system are plotted in Fig. 12 and show that the observed steep array of data points can be reproduced using plausible initial and final values of quartz and feldspar and assuming that feldspar exchanged ten times as fast as quartz in the case of the Horse Creek leucogranites, and twice as fast as quartz in the quartzite schist leucogranites. Isochrons for values for f_{qtz} of 0.3 and 0.6 are also shown, the former value corresponding closely to the slope of the array of the quartzite-schist leucogranite data. The steeper array for the Horse Creek leucogranites defines an isochron corresponding to a smaller f_{qtz} value, but the small number of data points precludes detailed analysis. A value of f_{qtz} of 0.3 corresponds to a kt value of ~0.35. A plausible range of empirically derived k_{qtz} values of 10^{-13} to 10^{-15} which is consistent with numerous other studies (Gregory et al. 1989) corresponds to a t of about 3.5×10^{12} to 3.5×10^{14} s or 0.1 to 10 Ma. This admittedly simple estimate brackets the estimate of duration of shear zone activity of 2.6 Ma of Hacker et al. (1990). The best correspondence between duration of fault movement and exchange is for a k_{qtz} value of $\sim10^{-14}$. A more detailed attempt to model the quartz-feldspar disequilibrium systematics is beyond the scope of this paper but these crude calculations show that it is possible that hydrothermal activity could have lasted for several million years, an estimate which is consistent with the duration of mylonitization as inferred from microstructural studies, though somewhat less than the long-term cooling history suggested by Ar-Ar geochronology (Dallmeyer et al. 1986).

The steeper exchange trajectory defined by the Horse Creek leucogranites compared with those in the quartzite-schist (Figs. 11 and 14) implies that there was a greater contrast in the rates of exchange of quartz and feldspar in the Horse Creek rocks ($k_{quartz}/k_{feldspar}$ ~0.1) than in the quartzite schist leucogranites ($k_{quartz}/k_{feldspar}$ ~0.5). It is possible that this reflects more intense dynamic recrystallization of quartz in the quartzite schist leucogranites, which would enhance the quartz exchange rate and bring it closer to that of feldspar. In the Horse Creek leucogranites, dynamic recrystallization may have been weaker because the surrounding, mechanically weak, carbonate mylonite accommodated most of the strain, at least to a greater extent than in the quartzite schist unit.

Conclusions

We have studied $^{18}O/^{16}O$ and D/H systematics in the vicinity of the detachment fault and underlying mylonite zone exposed at Secret Creek gorge, northern Ruby Mountains, Nevada, as well as the D/H systematics in high-grade rocks from several localities throughout this area. Because the aqueous fluids that infiltrated the fault zone environment had a very distinctive oxygen and hydrogen isotope composition, they left a very recognizable isotopic signature in the rocks through which they flowed, allowing their movement to be tracked in considerable detail. In particular, we have direct evidence for penetration of local meteoric water *at least* 70 m into rocks of the lower plate *at the time that they were being plastically deformed* at depths of 5–10 km below the surface. The most important results of this study are as follows.

1) Extremely low $\delta^{18}O$ values are observed in quartzite and leucogranite mylonites from the lower plate ductile shear zone exposed at Secret Creek gorge. In the virtually monomineralic quartzites, $\delta^{18}O$ decreases from values $\sim +12$ to values as low as $+2$ to $+8$ per mil and even lower in some of the pelitic schist mylonites (-0.1). Low-^{18}O mylonites occur throughout the Secret Creek gorge section, at depths to at least 70 m below the detachment surface. All biotite samples from the Secret Creek mylonites have uniformly low δD values of ~ -150 per mil.

2) The $\delta^{18}O$ values of low-grade, upper-plate rocks are variable. Vein quartz and calcite have extremely low values close to zero, while higher values are preserved in fine-grained matrix material.

3) Biotite and hornblende from localities throughout the northern Ruby Mountains (other than Secret Creek gorge) have variable δD values including some very low values (lower than -150), mostly for samples collected near fault zones. These findings suggest that small quantities of meteoric water penetrated these rocks over a wide area.

4) Fluid inclusion water in a sample of unstrained quartz from a breccia has a δD of -119, close to the value of present-day and Tertiary local meteoric water. The Secret Creek biotites would have been in equilibrium with water of similar isotopic composition at moderate temperatures of 480–620° C, similar to estimated temperatures of mylonitization.

5) The low $\delta^{18}O$ values observed for the quartzites are consistent with isotopic exchange with meteoric water. Because quartz is very resistant to exchange, this interaction must have occurred at high temperatures (>400° C) or during dynamic recrystallization.

6) The low $\delta^{18}O$ values are spatially associated with the detachment fault zone and its underlying mylonites. Taken with the evidence that even quartz experienced major ^{18}O-depletion, and in the absence of a cataclastic breccia zone, this suggests that meteoric water infiltration accompanied mylonitization.

7) Independent temperature estimates of mylonitization from mineral equilibria are 580–620° C. At these temperatures, the lowest $\delta^{18}O$ quartzites would have been in equilibrium with a meteoric water with a value of $\sim +1.5$ per mil. This is a plausible value for local meteoric water that has become ^{18}O-enriched by interaction with high-^{18}O upper plate rocks.

8) Analysis of the quartz-feldspar disequilibrium systematics observed in leucogranite mylonites suggests that exchange lasted 0.1–10 Ma, consistent with independent estimates from microstructural data for the duration of deformation.

Acknowledgements. This research was in part supported by NSF grants EAR8720097 and EAR9019256 to SMW and EAR9005717 to JRO. Henry Fricke acknowledges support from the Richter Fund for Undergraduate Research at the University of Chicago. We are grateful to Mark Peters, Eriks Puris, R.N. Clayton, and T.K. Mayeda for discussions and laboratory assistance, to J.M. Ferry, A.M. McCaig and R. Kerrich for reviews, and to James Eason for typing the manuscript.

References

Bickle MJ, McKenzie D (1987) The transport of heat and matter by fluids during metamorphism. Contrib Mineral Petrol 95:384–392

Blattner P, Lassey KR (1989) Stable isotope exchange fronts, Damköler numbers and fluid to rock ratios. Chem Geol 78:381–392

Buck WR (1988) Flexural rotation of normal faults. Tectonics 7:959–973

Chiba H, Chacko T, Clayton RN, Goldsmith JR (1989) Oxygen isotope fractionations involving diopside, forsterite, magnetite, and calcite: application to geothermometry. Geochim Cosmochim Acta 53:2985–2995

Clayton RN, O'Neil JR, Mayeda TK (1972) Oxygen isotope exchange between quartz and water. J Geophys Res 77:3057–3067

Clayton RN, Goldsmith JR, Mayeda TK (1989) Oxygen isotope fractionations in quartz, albite, anorthite, and calcite. Geochim Cosmochim Acta 53:725–733

Craig H (1961) Isotopic variations in meteoric waters. Science 133:1702–1703

Criss RE, Taylor HR Jr (1986) Meteoric-hydrothermal systems. In: Valley JW, Taylor HP Jr, O'Neil JR (eds) Stable isotopes in high temperature geological processes. Rev Mineral 16:373–424

Criss RE, Gregory RT, Taylor HP Jr (1987) Kinetic theory of oxygen isotope exchange between minerals and water. Geochim Cosmochim Acta 51:1099–1108

Dallmeyer RD, Snoke AW, McKee EH (1986) The Mesozoic-Cenozoic tectonothermal evolution of the Ruby Mountains-East Humboldt Range, Nevada: a cordilleran metamorphic core complex. Tectonics 5:931–954

Davis SH (1980) Structural characteristics of metamorphic core complexes, southern Arizona. Geol Soc Am Mem 153:35–78

Dokka RK, Mahaffie MJ, Snoke AW (1986) Thermochronologic evidence of major tectonic denudation associated with detachment faulting, northern Ruby Mountains-East Humboldt Range, Nevada. Tectonics 5:995–1006

England PC, Richardson SW (1977) The influence of erosion upon mineral facies of rocks from different metamorphic environments. J Geol Soc London 134:201–213

Etheridge MA, Wall VJ, Cox SF (1984) High fluid pressure during regional metamorphism and deformation: implications for mass transport and deformation mechanisms. J Geophys Res 89:4344–4358

Etheridge MA, Wall VJ, Vernon RH (1983) The role of the fluid phase during regional metamorphism and deformation. J Metamorph Geol 1:205–226

Friedman I, O'Neil JR (1977) Compilation of stable isotope fractionation factors of geochemical interest. US Geol Survey Prof Pap 440-KK

Giletti BJ (1985) The nature of oxygen transport within minerals in the presence of hydrothermal water and the role of diffusion. Chem Geol 53:197–206

Giletti BJ, Yund RA (1984) Oxygen diffusion in quartz. J Geophys Res 89:4039–4046

Gregory RT, Criss RE (1986) Isotopic exchange in open and closed systems. In: Valley JW, Taylor HP Jr, O'Neil JR (eds) Stable isotopes in high temperature geological processes. Rev Mineral 16:91–127

Gregory RT, Criss RE, Taylor HR Jr (1989) Oxygen isotope exchange kinetics of mineral pairs in closed and open systems: application to problems of hydrothermal alteration of igneous rocks and Pre-Cambrian iron formations. Chem Geol 75:1–42

Hacker BR, Yin A, Christie JM, Snoke AW (1990) Differential stress, strain rate, and temperatures of mylonitization in the Ruby Mountains, Nevada: implications for the rate and duration of uplift. J Geophys Res 95:8569–8580

Hurlow HA, Snoke AW, Hodges KV (1991) Temperature and pressure of mylonitization in a Tertiary extensional shear zone, Ruby Mountains-East Humboldt Range, Nevada: Tectonic implications. Geology 19:82–86

Kerrich R (1988) Detachment zones of Cordilleran metamorphic core complexes: thermal, fluid and metasomatic regimes. Geol Rundschau 77:157–182

Kerrich R, Hyndman D (1986) Thermal and fluid regimes in the Bitteroot lobe Sapphire block detachment zone, Montana: Evidence from $^{18}O/^{16}O$ and geologic relations. Geol Soc Am Bull 97:147–155

Kerrich R, Rehrig W (1987) Fluid motion associated with Tertiary mylonitization and detachment faulting: $^{18}O/^{16}O$ evidence from the Picacho metamorphic core complex, Arizona. Geology 15:58–62

Kistler RW, Ghent ED, O'Neil JR (1981) Petrogenesis of garnet two-mica granites in the Ruby Mountains, Nevada. J Geophys Res 86:10591–10606

Knipe RJ (1989) Deformation mechanisms – recognition from natural tectonites. J Struct Geol 11:127–146

Koons PO (1987) Some thermal and mechanical consequences of rapid uplift: an example from the Southern Alps, New Zealand. Earth Planet Sci Lett 86:307–319

LaTour TE, Barnett RL (1987) Mineralogical changes accompanying mylonitization in the Bitteroot dome of the Idaho batholith: Implications for timing of deformation. Geol Soc Am Bull 98:356–363

Lister GS, Snoke AW (1984) S-C mylonites. J Structural Geol 6:617–638

Matsuhisa T, Goldsmith JR, Clayton RN (1979) Oxygen isotope fractionation in the system quartz-albite-anorthite-water. Geochim Cosmochim Acta 43:1131–1149

McCaig AM (1984) Fluid-rock interaction in some shear zones from the Central Pyrenees. J Metamorph Geol 2:129–141

McCaig AM (1988) Deep fluid circulation in fault zones. Geology 16:867–870

McCaig AM, Wickham SM, Taylor HP Jr (1990) Deep fluid circulation in Alpine shear zones, Pyrenees, France; field and oxygen isotope studies. Contrib Mineral Petrol 106:41–60

McCrea JM (1950) On the isotopic chemistry of carbonates and a paleotemperature scale. Chem Phys 18:849–857

Miller EL, Gans PB, Garing J (1983) The Snake range decollement: an exhumed mid-Tertiary ductile-brittle transition. Tectonics 2:239–263

Noble LF (1941) Structural features of the Virgin Spring area, Death Valley, California. Geol Soc Am Bull 52:941–1000

Norton D (1984) A theory of hydrothermal systems. Ann Rev Earth Planet Sci 12:155–177

O'Neil JR (1987) Preservation of C, H, O isotopic ratios in the low temperature environment. In: Kyser TK (ed) Stable isotope geochemistry of low temperature fluids. MAC Shortcourse Handbook, vol 13, pp 85–128

O'Neil JR, Silberman ML (1974) Stable isotope relations in epithermal Au-Ag deposits. Econ Geol 69:902–909

O'Neil JR, Clayton RN, Mayeda TK (1969) Oxygen isotope fractionation in divalent metal carbonates. J Chem Phys 51:5547–5558

Peters MT, Wickham SM (1989) Petrographic and petrologic evidence for high-temperature fluid infiltration in the East Humboldt Range, northeastern Nevada. Geol Soc Am Abstr with Progr 21:327

Rehrig WA, Reynolds SJ (1980) Geologic and geochronologic reconnaissance of a northwest-trending zone of metamorphic core complexes in southern and western Arizona. In: Crittenden MD, Coney PJ, Davis GH (eds) Cordilleran metamorphic core complexes. Geol Soc Am Mem 153:131–158

Reynolds SJ, Lister GS (1987) Structural aspects of fluid-rock interactions in detachment zones. Geology 15:362–366

Roddy MS, Reynolds SJ, Smith BM, Ruiz J (1988) K-metasomatism and detachment-related mineralization, Harcuvar Mountains, Arizona. Geol Soc Am Bull 100:1627–1639

Sharma T, Clayton RN (1965) Measurement of $^{18}O/^{16}O$ ratios of total oxygen from carbonates. Geochim Cosmochim Acta 29:1347–1353

Sharp ZD, O'Neil JR, Essene EJ (1988) Oxygen isotope variations in granulite-grade iron formations: constraints on oxygen isotope diffusion and retrograde isotopic exchange. Contrib Mineral Petrol 98:490–501

Sheppard SMF, Nielsen RL, Taylor HP Jr (1969) Oxygen and hydrogen isotope ratios of clay minerals from porphyry copper deposits. Econ Geol 64:755–777

Sheppard SMF (1986) Characterization and isotopic variations in natural waters. In: Valley JW, Taylor HP Jr, O'Neil JR (eds) Stable isotopes in high temperature geological processes. Rev Mineral 16:165–183

Sibson RH (1983) Continental fault structure and the shallow earthquake source. J Geol Soc London 140:747–767

Sibson RH, Moore JMM, Rankin AH (1975) Seismic pumping – hydrothermal fluid transport mechanism. J Geol Soc Lond 131:653–659

Smith BM, Reynolds SJ, Day HW, Bodnar RJ (1991) Deep-seated fluid involvement in ductile-brittle deformation and mineralization, South Mountains metamorphic core complex, Arizona. Geol Soc Am Bull 103:559–569

Snoke AW (1980) Transition from infrastructure to suprastructure in the northern Ruby Mountains, Nevada. In: Crittenden MD, Coney PJ, Davis GH (eds) Cordilleran metamorphic core complexes. Geol Soc Am Mem 153:287–333

Snoke AW, Howard KA (1984) Geology of the Ruby Mountains-East-Humboldt Range Nevada – a Cordilleran metamorphic core complex. In: Lintz Jr (ed) Western geological excursions, vol 4. Geological Society of America 1988 Annual Meeting, Reno, Nevada, pp 260–303

Snoke AW, Lush AP (1984) Polyphase Mesozoic-Cenozoic deformational history of the northern Ruby Mountains-East Humboldt Range, Nevada. In: Lintz J Jr (ed) Western geological excursions. Geological Society of America 1988 Annual Meeting, Reno, Nevada, pp 232–260

Snoke AW, McGrew AJ, Valasek PA, Smithson SB (1990) A crustal cross-section for a terrain of superimposed shortening and extension: Ruby Mountains-East Humboldt Range metamorphic core complex, Nevada. In: Salisbury MH, Fountain DM (eds) Exposed cross sections of the continental crust. Kluwer Academic Publishers, Boston, pp 103–135

Suzuoki T, Epstein S (1976) Hydrogen isotope fractionation between OH-bearing silicate minerals and water. Geochim Cosmochim Acta 40:1229–1240

Taylor HP Jr, Epstein S (1962) Relationships between $^{18}O/^{16}O$ ratios in coexisting minerals of igneous and metamorphic rocks.

Part I: principles and experimental results. Bull Geol Soc Am 73:461–480

Taylor HP Jr (1977) Water/rock interactions and the origin of H_2O in granitic batholiths. J Geol Soc Lond 133:509–558

Wickham SM, Taylor HP Jr, Snoke AW (1987) Fluid-rock-melt interaction in metamorphic core complexes; a stable isotope study of the Ruby Mountains-East Humboldt Range, Nevada. GSA Abstr with Progr 19, 463

Wickham SM, Peters MT (1990) An oxygen isotope discontinuity in high-grade rocks of the East Humboldt Range, Nevada. Nature 345:150–153

Wickham SM, Taylor HP Jr, Snoke AW, O'Neil JR (1991) An oxygen and hydrogen isotope study of high-grade metamorphism and anatexis in the Ruby Mountains-East Humboldt Range Core Complex, Nevada. In: Taylor HP Jr, O'Neil JR, Kaplan IR (eds) Stable isotope geochemistry: a tribute to Samuel Epstein. The Geochemical Society, Special Publication No. 3, pp 373–390

Willden R, Kistler RW (1969) Geologic map of the Jiggs Quadrangle, Elko County, Nevada. US Geological Survey Map GQ-859, Washington, DC

Wright JE, Snoke AW (1986) Mid-Tertiary mylonitization in the Ruby Mountain-East Humboldt Range metamorphic core complex, Nevada. Geol Soc Am Abstr with Progr 18:795

Wright LA, Troxel BW (1973) Shallow-fault interpretation of Basin and Range structure, southwestern Great Basin. In: de Jong KA, Scholton B (eds) Gravity and tectonics. Wiley, New York, pp 397–407

Yin A (1989) Origin of regional, rooted low-angle faults: a mechanical model and its tectonic implications. Tectonics 8:469–482

Editorial responsibility: J Ferry